2011

Multiphysics Modeling of Biomolecular Detection Process Using SiNW sensors at Ultralow Concentration with Electrokinetic Effects

Qingjiang Guo
Lehigh University

Multiphysics Modeling of Biomolecular Detection Process Using SiNW sensors at Ultralow Concentration with Electrokinetic Effects

by

Qingjiang Guo

A Thesis

Presented to the Graduate and Research Committee

of Lehigh University

in Candidacy for the Degree of

Master of Science

in

Mechanical Engineering and Mechanics

Lehigh University

July 2011

Thesis is accepted and approved in partial fulfillment of the requirements for the Master of Science.

Date

Dr. Yaling Liu
Thesis Advisor

Dr. D. Gary Harlow
Chairperson of the Department

Acknowledgments

Throughout the duration of my two-year graduate life, I have been very fortunate in being surrounded by many supportive friends and colleagues. This thesis is a culmination of their time and efforts and would not have been made possible without their kind advice and help.

The long list of my indebtedness begins with my advisor, Professor. Yaling Liu, whose continual encouragement and inspired guidance enable me to overcome many difficulties, both research-related and personal, and succeed in completing the work presented in this thesis. I will always keep his suggestion “There is always an easy way to solve any difficulties” in mind and continue to grow and become a professional.

I would also like to express my gratitude to all members in Nanoscale Integration Lab in University of Texas at Dallas. They have all helped with perceptive questions and timely suggestions of new areas for investigation. Professor Walter Hu, in particular, has devoted numerous efforts in keeping track of collaborations and sharing experimental experiences. In addition, I am grateful for constructive discussions with many others, particularly Ruhai Tian and Li Tao.

Many thanks are given to my office and lab mates, Samar Shah, Abhijit Ramchandran, Manohara Mariyappa, Jifu Tan, Antony Thomas and Annas Shah for their general willingness to share and discuss research problems and life experiences and their ability to tolerate my immature behavior in this young and growing group.

I thank professors and classmates in Packard Laboratory in Lehigh University. I really appreciate the time we spent together to learn new knowledge and solve puzzles

together. The specific assistance of my GTA advisor Charles R. Smith served to smooth out many of the challenges I faced during the process of being a good teaching assistant. And the inspired discussions with my classmate Siming Zhang helped me successfully pass the final exam of the course “Fundamental of Solid Mechanics”.

Thank you to my collective roommates over the past two years Phillip Snow, Yu Zhang, Xiaonan Li and others. Thanks for helping me accommodate to the life in USA. Phillip, thank you especially for bringing me involved in American culture.

Finally, I would like to thank my family, who always serves as a true mainstay from start to finish, despite thousands of miles away. I appreciate all the sacrifices they have made to provide opportunities and chances to enrich my life experience. I would also like to thank God for always being by my side. I know I would not have accomplished so much without Him.

Contents

List of Tables

List of Figures

Abstract

SiNW sensors, due to their ultrasensitivity, selectivity, and label-free and real-time detection capabilities, are emerging as a promising tool in quantification and analysis of biochemical processes. In the past several decades, SiNW sensors have been widely applied in detecting DNA, proteins, virus, gas molecules and many other biomolecules. Despite these advancements, the molecular-level understanding of bio-nano interface and interaction of SiNW sensing system is still very limited, especially at ultralow concentration (~ fM), which has hindered the understanding of experimental results as well as biosensor design. One example is the large discrepancy in detection time (three orders of magnitude difference) between experimental demonstration of silicon nanowire (SiNW) sensors and the theoretical diffusion-reaction model. Another example is that the understanding of biomolecular dynamics under applied field conditions such as electric field or magnetic field is lacking and has never been applied to emerging biosensors such as nanowire bio-FETs. The goal of this thesis is to reveal the puzzling detection process of biomolecules at ultralow concentration and explore possible contribution of electrokinetic effects on detection speed.

The basic principle of biomolecular detection using SiNW sensors is to convert the information of biological interactions on SiNW surfaces into an observable electronic signal. Biological receptors on nanowire surfaces could recognize the target biomolecules in the buffer solution due to their high specificity and strong binding affinity. This target-receptor interaction changes the surface potential of SiNW, and thus modulates the conductance of devices and triggers an electrical signal. To detect this electric field

variance, a solution gate is usually used to set the nanowire in a range that is sensitive to changes of surface potential. The applied voltage on solution gate would induce electric field and biomolecules in the SiNW sensors would be subject to electrokinetic effects, which are proposed to account for the discrepancy of detection time at ultralow concentration.

Here, a novel multiphysics computational model is developed to study the physical mechanism of biomolecular detection process at ultralow concentration for SiNW biosensors. The electrokinetic effects, including electrophoretic force and electroosmotic flow, have been studied under various conditions systematically. Considering electrokinetic effects in a typical SiNW sensor with a single nanowire, the detection time decreases over ninety times for charged biomolecules and over forty times for uncharged biomolecules. The design considerations of SiNW sensor, including nanowire design, solution gate design and biomolecular charge, are also studied using the developed computational approach. The size and number of nanowires, gate voltage and biomolecular charge can lead to significant reduction of detection time, while the position of solution gate doesn’t have any effect on biomolecular detection process. Appropriate combinations of the SiNW design and electrokinetic effects could provide a satisfactory explanation to detection time discrepancy between experiments and diffusion-reaction theory at ultralow concentration. This work provides deep insights to the mechanism of biomolecular detection process and could be used to guide the design optimization of SiNW sensing devices.

Chapter 1

Introduction

This thesis reports a novel multiphysics computational model for SiNW biosensors (also called silicon nanowire field-effect transistors or SiNW-FETs), which are used to analyze biological interaction processes by converting biological events into electronic signal. Recently, SiNW biosensors attract tremendous attentions as a promising tool in biosensor design because of their ultrasensitivity, selectivity, and label-free and real-time detection capabilities [1-2]. In this chapter, a brief introduction to biomolecular detection is provided, followed by the descriptions of electrochemical biosensing and a summary of some currently-used electrochemical biosensors. Field-effect transistor-based biosensors are then discussed along with some current techniques. Particularly, SiNW sensors, which are attracting huge amount of efforts nowadays, are described in detail in separated sections. The chapter ends with a generic scope of this thesis, including chapter summaries.

1.1 Biomolecular detection

The ability to quantify and analyze biologically significant molecules in biological systems has tremendous impacts for biomedical applications and cellular programming investigation. Early disease detection, glucose monitoring, DNA sequencing and many other areas all depend on accurate quantification and analysis of biological solutions. During the last two decades, biosensor-related research has experienced explosive growth. Various biosensing techniques are developed to detect biomolecules such as

DNA, RNA, and especially proteins with high sensitivity and selectivity, both for laboratory use and lab-on-a-chip applications. The ultimate goal of biomolecular detection is to perform fast, sensitive and quantitative detection of target biomolecules in a biological sample. In addition, the ability to detect multiple biomolecules simultaneously in a single, versatile detection platform is also desirable, which is referred to as high-throughout biosensing. At present, many efforts have been devoted into developing biomolecular detection techniques and significant advancements have been achieved, which brings the state-of-the-art closer to the goal.

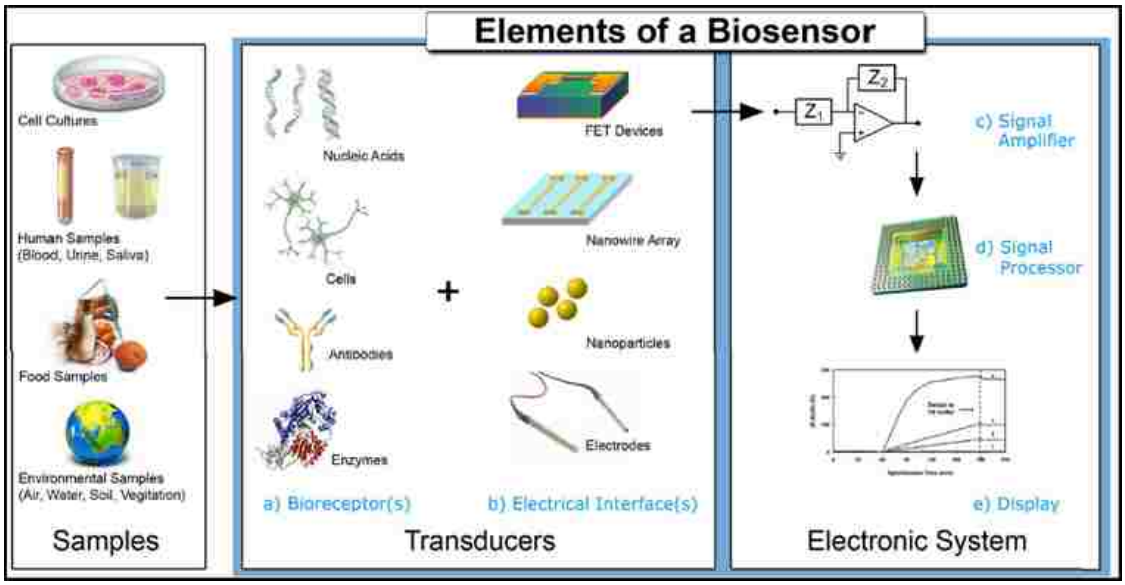

Figure 1.1: The construction of a typical biosensor with elements and selected components [4].

A generic biosensor contains two parts, a chemical (molecular) recognition system and a physicochemical transducer [3]. The biological recognition system translates information from the biochemical domain, usually the concentration of certain specific analyte, such as ligands, enzyme and complementary part of DNA, into a chemical or physical output signal with a defined sensitivity. The transducer part of the sensor serves

to transfer the signal from the output domain of the recognition system into an analytically useful signal. Figure 1.1 shows schematically the parts comprising a typical biosensor: a) conjugate receptors that are used to capture target biomolecules; b) an interface architecture for biological interactions and signal generation picked up by c) the transducer element, which could convert the transducer signal, such as the in-coupling angle of a laser beam, current produced at an electrode, to an electronic signal, which would be sent for processing by d) computer software to be converted to a meaningful physical parameter; finally, the resulting quantity has to be presented through e) an interface to the human operator [4].

The biosensing approaches could be classified into two major categories, one is the optical sensing techniques, and the other is the electrochemical techniques, both of which allow for real-time, in situ, non-destructive and label-free analysis of biological solutions. Some commonly used optical biosensing methods include fluorescence microscopy, ellipsometry, surface plasmon resonance and the quartz crystal microbalance, as described below.

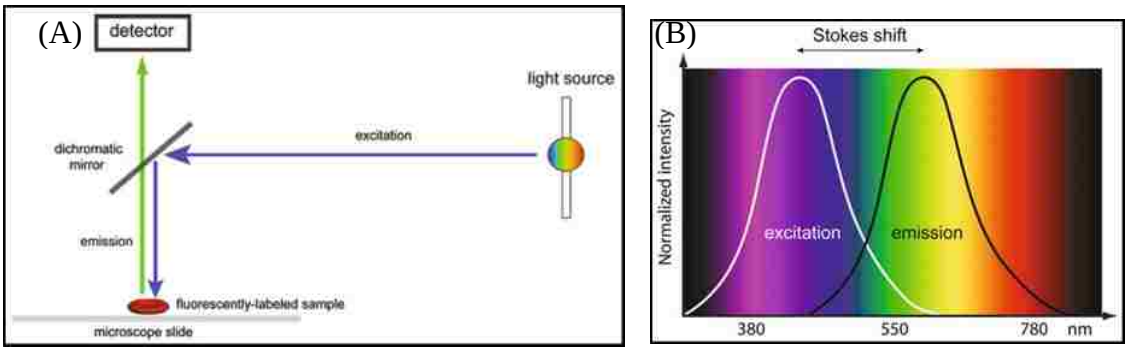

Figure 1.2: (A) Diagram illustrating the basic principle of fluorescence microscopy; (B) Comparison of excitation and emission spectra of a hypothetical fluorescent molecule. [5]

A fluorescence microscopy is an optical microscope used to study the properties of organic or inorganic substances using the phenomena of fluorescence instead of reflection and absorption [5-6]. Figure 1.2(A) shows the basic principle of a fluorescence microscopy. The light source emits light that is reflected by the dichromatic mirror through the objective into the sample. The fluorochromes present in the sample following excitation emit light of longer wavelength (fluorescence) that goes back through the objective and dichromatic mirror and form the final image on a detector [5]. The difference between excitation and emission spectra is illustrated in Figure 1.2(B). Fluorescence microscopy can perform extremely sensitive measurements, the detection limits of which could reach analyte concentration zeptomole (10^{-21} moles) [7] and yoctomole (10^{-23} moles) [8]. However, this technique requires label target biomolecules with other enzymes [9], DNA [10] or inorganic compounds [11-12], to reveal a detection signal under fluorescence microcopy. Labeling biomolecules is a trivial work, and the original behaviors of biomolecules would possibly be changed, which consequently makes accurate quantification detection difficult.

Ellipsometry uses optical technique to measure the change of ellipsometric angles in polarization state of light reflected from the surface of a sample and then the optical properties, thickness, morphology or roughness [13-14] of layers for films and amount of adsorbed protein [15-16] on the surface can be calculated. Surface plasmon resonance (SPR) is based on refractive index changes due to the effect of the interface between metal and the external medium on the propagation of electromagnetic waves [17-18]. The changes in the refractive index can be induced by the presence of biomolecules and the surface concentration or mass coverage can then be calculated using the de Feijter

formula [19]. Quartz crystal microbalance (QCM) is a mass detector whose operation is based on measuring changes in the resonance frequency and dissipation factor of an oscillating quartz crystal upon adsorption of a viscoelastic layer [20-21]. The oscillation is based on the piezoelectric effect and the crystals typically have a fundamental resonance frequency of 5 MHZ, which decreases upon mass adsorption.

One disadvantage of the above optical sensing techniques is the difficulty to miniaturize these sensing devices, both down in size and up in number, which makes them cost-expensive and, most importantly, not suitable for multiplex detection for a single biological sample. Electrochemical biosensors, which convert biological information directly into electronic signals, have the potential to overcome this drawback, as described in section 1.2.

1.2 Electrochemical biosensors

An electrochemical biosensor, as defined by the International Union of Pure and Applied Chemistry (IUPAC), is a self-contained integrated device, which allows biomolecular detection through a biological recognition element (or biochemical receptor) in direct spatial contact with an electrochemical transduction element [4]. Different from optical sensors that require numerous time and efforts to use microscopes or other devices to process the biological binding events, an electrochemical biosensor provides an attractive platform to quantify and analyze the biological samples through direct conversion of biological information to electronic signals, thus allowing more rapid and convenient sensing detection. Some inherent advantages of electrochemical biosensors include low-cost production, friendly interface, easy miniaturization, excellent

detection limits, also with small analyte volumes and ability to combine with other sensing approaches [22].

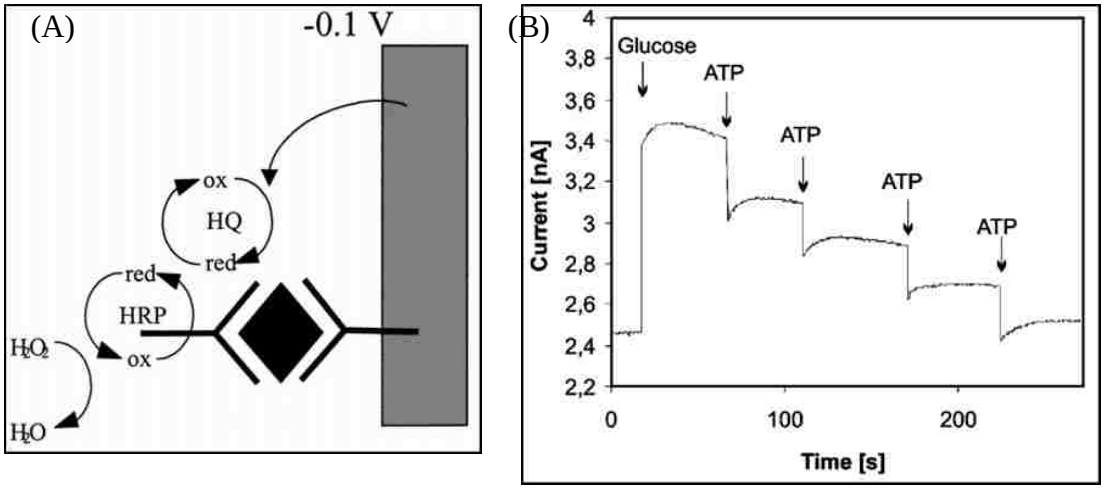

Figure 1.3: (A) Schematic illustration of the mechanism of the amperometric detection of H_2O_2 using HRP [24]; (B) Hydrodynamic response of a biosensor after continuing adding ATP to consume the glucose [25].

According to the mode of signal transduction, electrochemical sensors could be classified as amperometric, potentiometric, field-effect or conductivity sensors. Amperometry is based on the measurement of the current resulting from the electrochemical oxidation or reduction of an electroactive species [14]. During the experiments, a constant potential is often maintained at a Pt-, Au- or C-based working electrode or an array of electrodes with respect to a reference electrode. Therefore, the measured current is directly correlated to the bulk concentration of the electroactive species or its production or consumption rate within the adjacent biocatalytic layer. As biocatalytic reaction rates are often chosen to be first-order dependent on the bulk analyte concentration, such steady-state currents are usually proportional to the bulk analyte concentration. The simplest forms of amperometric biosensors are the Clark oxygen electrodes, which detect the reduction of oxygen at a working electrode at a constant

potential and generate a current proportional to oxygen concentration [23]. Another application of amperometry is to use an amperometric immunosensor based on a rigid immunocomposite to measure human chorionic gonadotropin β-subunit (β-HCG), as shown in Figure 1.3(A). β-HCG is determined with a sandwich assay using anti-b-HCG conjugate labeled with horseradish peroxidase (HRP). The extent of the immunological interaction is quantified by the activity of the labeling enzyme: peroxidaseis regenerated after the enzymatic reduction of H_2O_2 by hydroquinone which is used as a mediator in the solution. The reduction of hydroquinone is amperometrically monitored using a potential of −0.1V [24]. In addition, Kueng *et al.* applied amperometric biosensing technique to detect adenosine-5'-triphosphate (ATP) by co-immobilization of the enzyme glucose oxidase (GOD) and hexokinase (HEX). The electrochemical signal, generated by the oxidation of H_2O_2 at the electrode surface in the presence of glucose, would decrease after adding ATP, which, together with HEX, would catalyze the enzymatic reaction [25]. A typical hydrodynamic response curve from amperometric measurements is shown in Figure 1.3(B) and the change in current response is proportional to the ATP concentration.

Another electrochemical biosensing technique is potentiometry. Potentiometric devices measures the potential difference between either an indicator and a reference electrode or two reference electrodes separated by a permselective membrane, when zero or no significant current flows between them [22, 26]. In other words, potentiometry provides information about ion activity in electrochemical reactions. The potential differences between these ions and the reference electrode are proportional to the logarithm of the ion concentration, as described by the Nernst-Donnan equation [27]:

$$E_{cell} = E_{cell}^{0} - \frac{RT}{nF} \ln Q \tag{1.1}$$

where E_{cell} is the cell potential at zero current, E_{cell}^{0} is a constant potential contribution to the cell, R is the universal gas constant, T is the absolute temperature in degrees Kelvin, n is the charge number of the electrode reaction, F is the Faraday constant and Q is the ratio of ion concentration at the anode to ion concentration at the cathode. The most common potentiometric devices are PH electrodes and this technique could also be applied to detect other ions, such as F^{-}, I^{-}, CN^{-}, Na^{+}, K^{+} and Ca^{2+}. Vigassy *et al.* constructed Ca^{2+}, Ag^{+} and Na^{+} selective electrodes using poly(styrene-co-divinylbenzene)-based monolithic capillaries of an inner diameter of 200 μm and a length of 2-5 mm and potentiometric responses down to 10^{-8} – 10^{-9} M solutions were achieved [28]. Guo *et al.* fabricated a ligand-free tridodecylmethylammonium chloride (TDMAC)-based polymeric membrane ion selective electrode to measure ascorbate by the activity of permanganate ions released at the sample-membrane phase boundary [29]. Currently, Smirnova *et al.* developed a micro-potentiometric sensor for detecting alkali ions (Na+, K+ and NH4+) based on external microelectrodes introduced into a microchip [30], the setup of which is shown in Figure 1.4(A). It contains three ISEs for three different types of alkali ions, and an Ag/AgCl electrode as the reference potential. The valve capillary is connected to a pump to provide constant flow rate. Figure 1.4(B) shows a calibration curve for the Na+ ISE, the potential of which increases proportionally to the concentration of Na+.

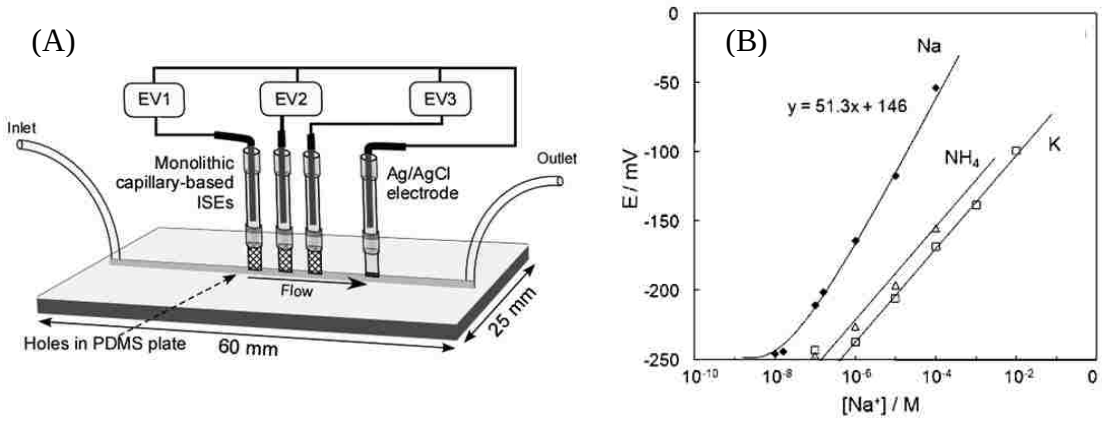

Figure 1.4: (A) Schematic of microchip setup of a potentiometric device; (B) Calibration curve of primary and interfering ions for Na^+-selective monolithic micro-ISEs. [30]

An important variation of the potentiometry systems used to determine ion concentrations in biological sample is the field-effect transistor (FET). Combined with the advantages of nanomaterials, FET-based devices would have the potential to reach the ultimate goal: ultrasensitive, selective, label-free and real time detection multiple biomolecules simultaneously, as described below.

1.3 Field-effect transistor-based biosensors

The FET is a type of transistor that uses an electric field to control the conductivity of a channel (a region depleted of charge carriers) between two electrodes (the source and drain) in a semiconducting material [4]. Usually, a FET is a three-electrode system, including source, drain and gate electrodes, as shown in Figure 1.5(A). The variance of the conductivity due to biological interactions would be transmitted to electric signals by the circuit composed of the source and drain electrodes. The gate electrode is used to modulate the electric field potential of the channel, which is made of semiconducting materials. Depending on the configuration and doping of the semiconducting materials,

the semiconductor would either attract charge carriers or repel charge carriers, resulting the change of the conductance between the source and drain electrodes. In the case of a p-type semiconductor, applying a negative gate voltage, which leads to negative charges at the interface between the gate electrode and dielectric, leads to an accumulation of carriers (positive holes) and a corresponding increase in conductance. On the other hand, applying a positive gate voltage to a p-type device, which leads to positive charges at the interface between the gate electrode and dielectric, depletes carriers in the device and lead to a decrease in the conductance [2].

The binding of a charged or chemical species to the semiconductor surface is analogous to applying a voltage on a gate. For example, when binding of a protein with net negative charge, such as DNA or RNA, to the surface of a p-Si FET, happens, an accumulation of positive hole carriers occurs, causing an increase in device conductance, as shown in Figure 1.5(B)(C) [2]. On the contrary, a decrease in the device conductivity would result from the depletion of charge carriers when positively charged biomolecules bind the p-Si FETs.

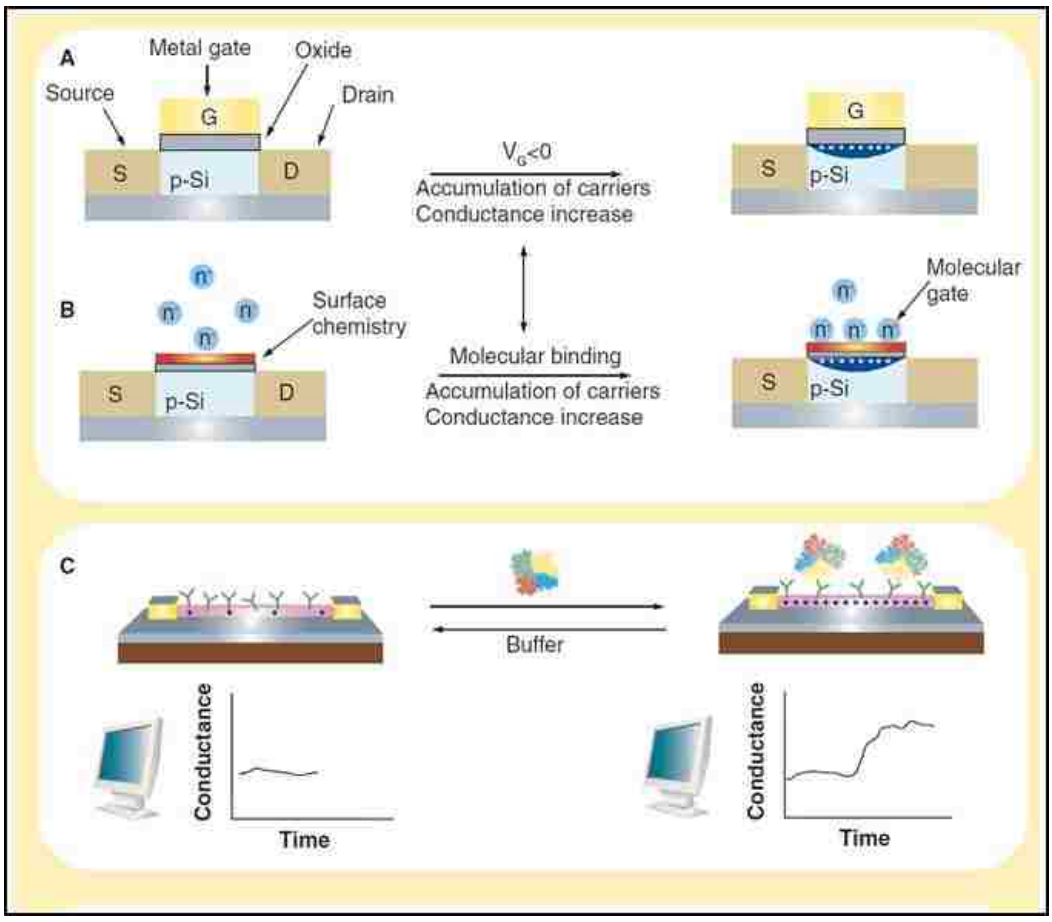

Figure 1.5: (A) Schematic of a field-effect transistor (FET) device consisting three electrodes, where source, drain and gate metal electrodes are represented by S, D and G, respectively; (B) Mechanism of the binding of a 'charged or polar' biological or chemical species to the chemically modified gate dielectric; (C) The conductance change of FET devices due to the binding events between receptors and target biomolecules. [2]

To date, a variety of FET-based biosensors has been employed for biological applications and they could be classified into three categories: enzyme-modified FETs (EnFETs), cell-based FETs, and immunologically functionalized FETs [1]. Enzyme-modified FETs are based on the immobilization of enzymes at the gate surface of pH-sensitive ion-selective-field-effect transistor (ISFET) and thus the immobilization process is critical to the devices' performance and sensitivity. In addition, in order to reduce

disturbing factors, such as temperature variance, light sensitivity and sensor drift, a pH ISFET/EnFET differential arrangement is employed, where the additional pH ISFET contains a blank enzyme-free membrane as a reference system [31-32]. The major applications of enzyme-modified FETs include urea, glucose and acetylcholine [26, 33-34]. Some typical problems about EnFET include the dependence of the sensor response on buffer capacity and ionic strength, the restricted dynamic measurement range and the non-linearity and the relatively slow response and recovery times. Cell-based FETs are based on the electrophysiological measurements of cells' metabolic products or extracellular potential and have been widely used for monitoring of electrical communication within neuronal networks and transmission paths of ionic channels [35-36], and detecting pharmaceutical agents, toxic substances and pollutants [37-38]. Immunologically functionalized FETs are highly related with immunological system. The electrodes are either immobilized with antibodies reacting with antigens in a biological sample, or immobilized antigens reacting with free antibodies. Currently, a variety of immunological biomolecules could be detected using immunologically functionalized FETs, such as β-bungarotoxin [39], proxidas [40], and herbicide simazine [41].

Due to the significant advancements in nanomaterials in the past two decades, FET nanostructure sensors have generated an enormous amount of interest for their potentials as a tool for highly sensitive detection. Traditional planar sensors (also called ISFETs), as shown in Figure 1.6(A), could only detect biomolecules down to concentration ~1 μM, because of the micro-scale size of sensing electrodes. Large number of binding events need occur to induce an observable conductance change. However, in FET nanostructure sensors, the source and drain electrodes are bridged by a nano-object instead of the planar

electrodes, as shown in Figure 1.6(B~D). These nanostructures, such as nanoparticles [42], nanowires [43], nanotubes [44], nanogaps and nanoscale films [45], have a high surface-to-volume ratio, which makes few biomolecular binding events enough to affect their bulk physical, chemical, or even electronic properties. In addition, some nanomaterials, such as silicon nanowire, could easily be modified with chemical biomolecules, which makes them perfect candidates for FET nanoscale sensing applications.

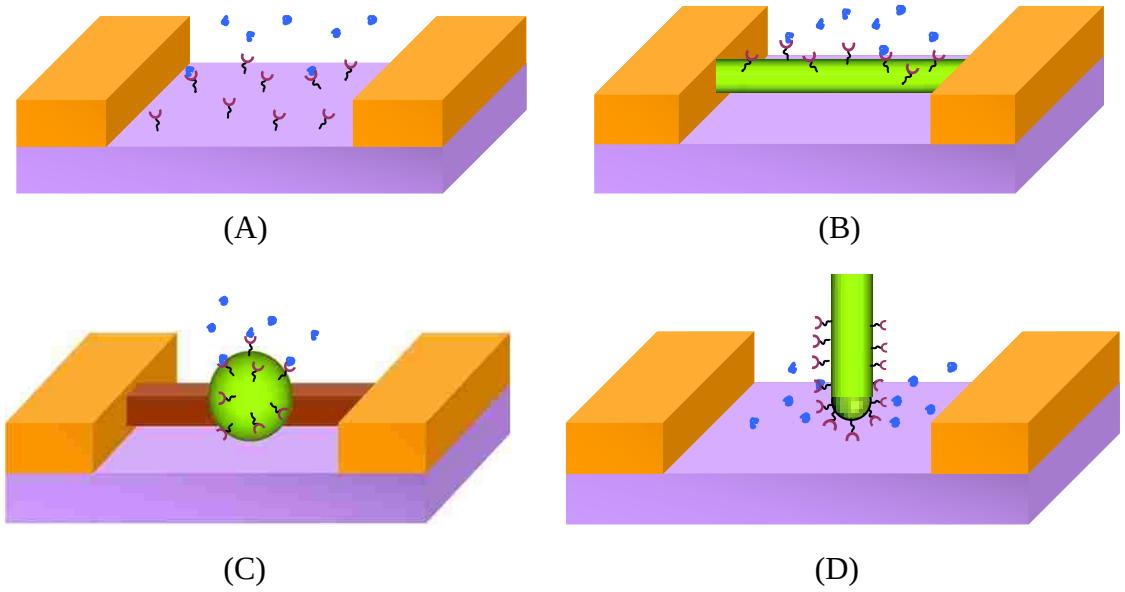

Figure 1.6: Schematic of different FETs: (A) Planar sensor, (B) FET-based nanowire sensor, (C) FET-based nanosphere sensor and (D) FET-based nanotip sensor.

Among these FET nanostructure sensors, CNTs, especially single-walled CNTs, are widely used in characterization of the antigen-antibody interactions [46-49], DNA hybridization [50-51] and enzymatic glucose detection [52]. Despite these advances of CNT-FETs in biosensing applications, there exist several shortcomings in the fabrication and applications of CNT-FETs. During the process of fabricating CNT-FETs, the

mixtures of semiconducting and metallic CNTs still hinder the future developments in nanoelectronics, and the detection mechanisms of CNT-FETs are somewhat complex and factors like field-effects, electron transfer, Schottky barriers should be considered [49, 51, 53-54]. On other hand, the sensing mechanism of SiNW-FETs is relatively straightforward and is determined by the variation of electric potential due to the biological interaction between target biomolecules and receptors on the nanowire surface.

1.4 Silicon nanowire field-effect transistors

Due to well-developed silicon industry, SiNW-FETs are emerging as a powerful and general platform for ultrasensitive, direct electrical detection of biological and chemical species. SiNWs, with different sizes [55-56], shapes [57], and dopants [58], could be precisely fabricated using the existing and mature silicon industry processing techniques. The structure of one of the best characterized examples of semiconducting nanowires can be prepared as single-crystal structures with diameter as small as 2-3 nm [55-56]. The attractive performances, such as high reproducibility [59], well-controlled electronic characteristics, make SiNW-FETs more appealing to use compared with CNT-FETs. In addition, due to nanoscale size of SiNWs, a few binding events could lead to obvious variations of the conductance of SiNWs. Therefore, the detection of single virus or biomolecule could become possible using SiNW-FETs.

Furthermore, due to the native oxide coatings on the silicon nanowire surface, the linkage of receptors is a straightforward and non-trivial thing. Previous data based on the research on planar chemical and biological arrays have already demonstrated the success of chemical modification of silicon oxide [60]. Another important point is the ability to

monitor the detection process in real-time, which could be used to characterize the dynamical process of biomolecular detection. SiNW-FETs are growing to be an ultrasensitive, real-time and multiplexed detection platform for medical and biological applications.

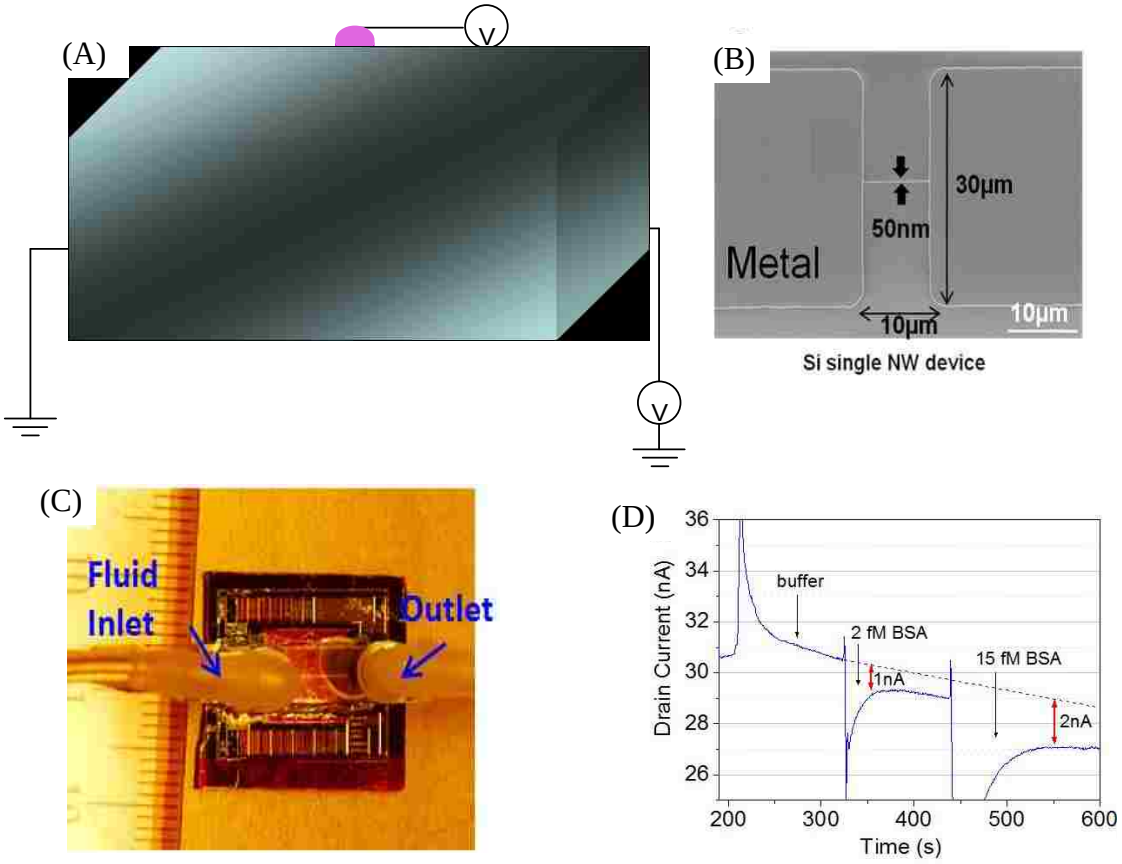

Figure 1.7: (A) Schematic of a typical SiNW sensor; (B) SEM image for SiNW sensor devices; (C) An integrated microchip for SiNW sensor; (D) Current change of SiNW devices at different concentrations of bovine serum albumin. [61-62]

A schematic sketch of a typical SiNW sensor is shown in Figure 1.7(A). A solution gate is used to modulate the conductance of the nanowire between two electrodes, which are used to transmit electronic signal. Biological interactions on the SiNW surface would vary the electric field potential, induce the conductance change of the device and an

electric signal would be observed. Figure 1.7(B) shows a SEM image of SiNW sensor on single crystalline Si on insulator (SOI) substrate. Figure 1.7(C) shows the finished sensor chip with sealed SU8 microchannels and connection with syringe pumps. As described before, SiNW sensor is characterized with high sensitivity and can detect target biomolecules at ultralow concentration, such as 2 fM, as illustrated in Figure 1.7(D) [61-62].

Among biosensors of various types, SiNW sensors are becoming the most sensitive and powerful devices for biological applications. Many efforts have been devoted to apply SiNW sensors to study biological interactions, such as protein-protein interactions, or protein-small molecule interactions. For example, Cui *et al.* functionalized SiNWs with biotin and studied the well-characterized ligand-receptor binding of biotin-streptavidin, and demonstrated the ability of SiNW sensor to detect streptavidin binding down to a concentration at least 10 pM [63]. Lin *et al.* studied the association of glutathione S-transferase-tagged calmodulin with a glutathione modified SiNW sensor and selective electric responses to Ca^{2+} (>= 1 mμM) and purified cardiac troponin I (approximately 7 nM) were achieved [64]. Another important application of SiNWs is to study DNA hybridization process. A commonly used receptor in DNA or RNA hybridization is the peptide nucleic acid (PNA), an artificially synthesized polymer similar to DNA. PNA doesn't have phosphate groups and thus electrostatic repulsion is weakened, which leads stronger binding of PNA/DNA or PNA/RNA strands than that of DNA/DNA or DNA/RNA duplexes. One representative example is that Hahm *et al.* modified the surfaces of SiNW devices with PNA to study wild type versus the ΔF508 mutation site in the cystic fibrosis transmembrane receptor gene and the concentration-

dependent measurements showed the detection could be carried out to at least the tens of femtomolar range [65].

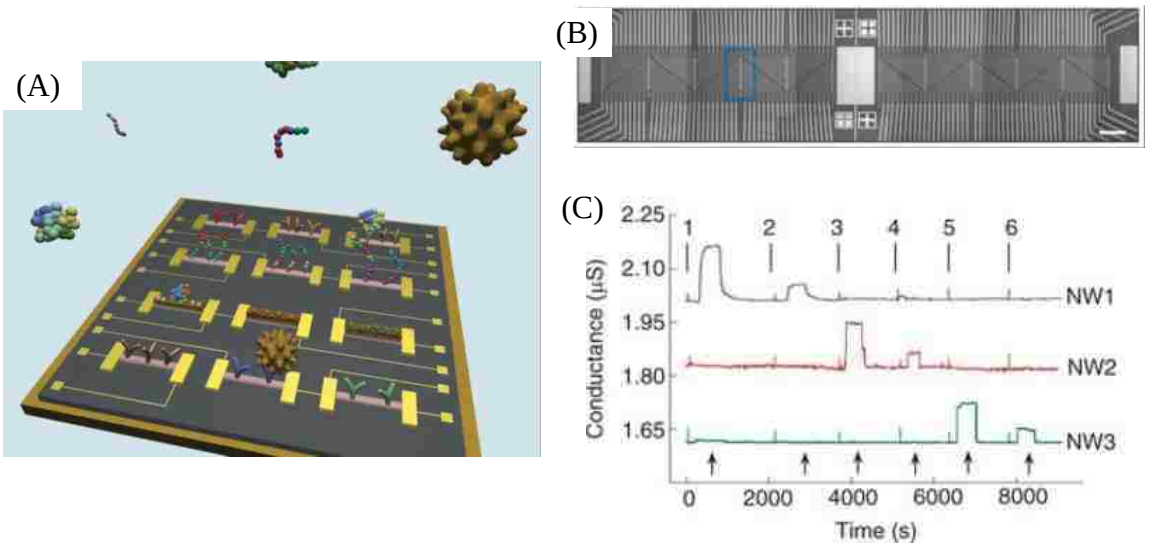

Figure 1.8: (A) Schematic of a nanowire device array for multiplexed, real-time sensing of multiple biological species; (B) Optical image of a portion of a nanowire array; (C) Simultaneous detection of PSA, carcinoembryonic antigen (CEA), and mucin-1 using NW1, NW2 and NW3 functionalized with corresponding antibodies. [66]

Furthermore, in the diagnosis of complex diseases, like cancer, would make the single-biomolecule test, such as analysis of prostate-specific antigen, inadequate. Therefore, it is especially important to detect multiple disease marker proteins simultaneously in a single versatile detection platform, and nanowire sensor arrays have the potential to address this challenge. Nanoscale size enables tens to hundreds of individually nanowire devices to be defined within a single microfluidic delivery channel and defining distinct surface receptors on different nanowire elements opens up the potential for multiplexed, real-time assays of multi-component solutions, as shown in Figure 1.8(A). Figure 1.8(B) shows the optical image of a nanowire sensor array containing more than 100 nanowire elements. Robust diagnosis of different biomolecules

with high selectivity is shown in Figure 1.8(C). Three nanowires are functionalized with monoclonal antibody receptors for PSA, CEA and mucin-1, respectively. As different protein solutions are sequentially delivered to the device array, clear signals are observed, which demonstrates the excellent capability of multiplexed real-time detection of biomolecules using nanowire array devices [66].

1.5 Fabrication of SiNW sensors

There are two major techniques for fabricating silicon nanowires: "top-down" and "bottom-up". The "top-down" method is to physically etch a single-crystalline silicon wafer using lithographic processes and electro-beam techniques [67]. On the other hand, the "bottom-up" method needs to grow SiNWs in a chemical vapor depositions (CVD) reaction and then assemble SiNW and fabricate electrodes through the photolithographic or electron-beam lithographic processes [68].

1.5.1 "Top-down" fabrication technique

The "top-down" fabrication technique is based on etching a single-crystalline silicon wafer through lithographic processes. Normally, silicon-on-insulator (SOI) wafer contains three layers, substrate Si wafer, buried silicon dioxide (thickness: 200 ~ 400 nm) and top Si layer (thickness 50 ~ 100 nm), as shown in Figure 1.9(A, i). SiNWs and corresponding electrodes can be fabricated through the standard procedures of photolithography, reactive ion etching (RIE), ion implantation, electron-beam lithography and thermal evaporation. The width of the SiNWs in SiNW sensors could reach the size of 100 nm.

Figure 1.9(A) illustrates a typical "top-down" process to fabricate SiNW biosensors. Firstly, the Si layer is doped with low-density boron or phosphorous of ~10^{15} cm^{-3}, which determines the semiconducting property and doping ratio of SiNWs. Secondly, the source and drain electrodes are defined by heavy doped area using a photomask design. Thirdly, RIE is used to etch the source and drain electrodes. Then nanoscale nanowire is fabricated with an electric-resist pattern and RIE etching. Subsequently, a thermal evaporation is used to make the contact leads and back-gate, and finally an insulator layer, such as Al_2O_3, SiO_2 and Si_3N_4, is coated on the SiNW biosensing devices [1].

The "top-down" procedure strongly relies on the high-resolution lithography (most of time it is electron-beam lithography), and thus it is more complex than the "bottom-up" method. In addition, the minimum width of the SiNWs using the "top-down" method could only reach ~100 nm. However, the "top-down" approach is totally based on standard semiconductor techniques and thus the device-array pattern could be precisely controlled and problems in positioning SiNWs could be avoided. Moreover, SiNWs of triangular section could be fabricated to reach the transverse dimension of less than 20 nm with the length of several micrometers [69].

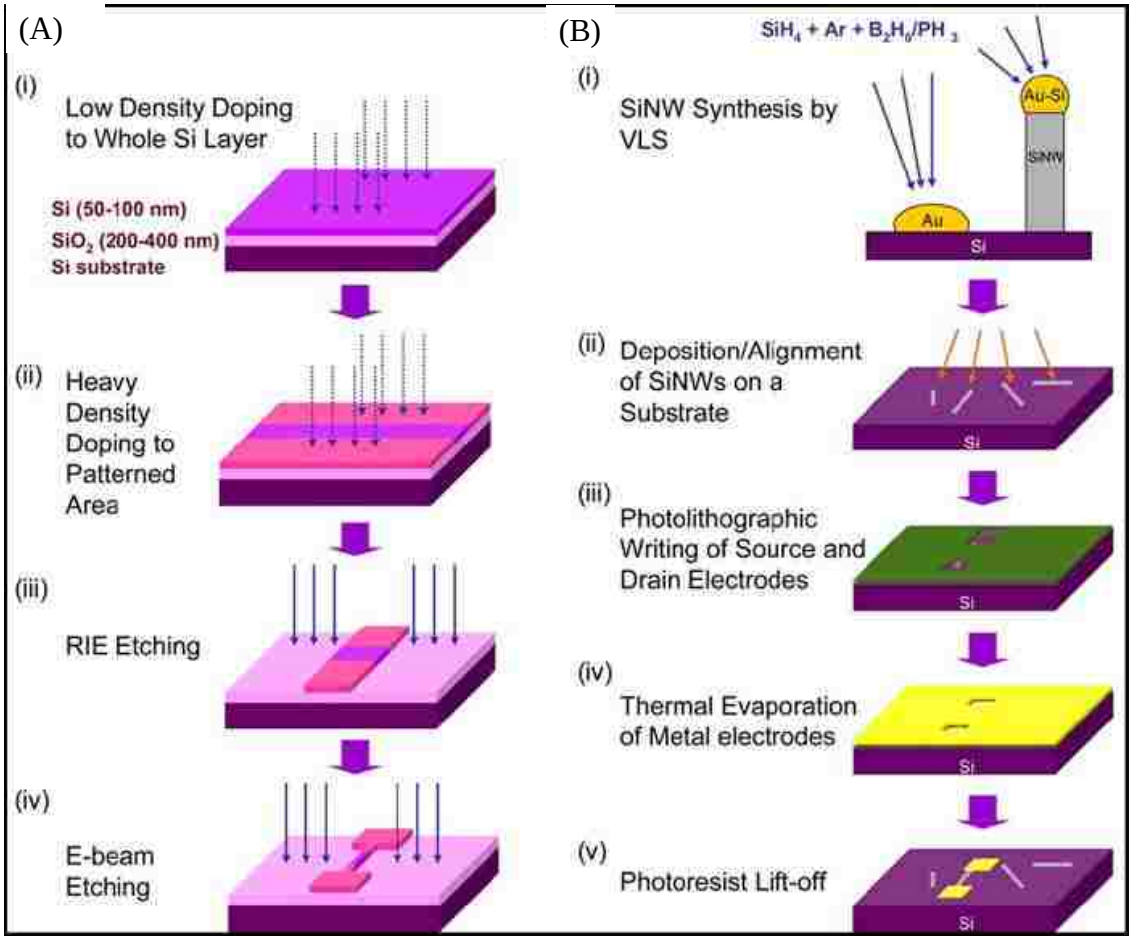

Figure 1.9: (A) Schematic illustration of a typical "top-down" process to fabricate SiNW sensors; (B) An illustration of a "bottom-up" method to fabricate SiNW sensors. [1]

1.5.2 "Bottom-up" fabrication technique

The "bottom-up" approach starts with the growth of SiNWs in a chemical vapor deposition (CVD) reaction via the vapor-liquid-solid (VLS) growing mechanism (Figure 1.9(B, i)) [70]. Usually, nanoparticles are added to catalyze the SiNW formation and control the size of SiNWs. Then synthesized SiNWs are randomly distributed on the substrate (Figure 1.9(B, ii)). The second step is to assemble these SiNWs deliberately (Figure 1.9(B, iii)), otherwise, the device fabrication would suffer from inefficient

fabrication yields, which could limit their development in the industrial applications. Several common used nanowire assembly techniques include flow-assisted alignment [71], Langmuir-Blodgett technique [59, 72-74], bubble-blown technique [75], electric-field-directed assembly [76-79], and smearing-transfer method [80]. To fabricate the source and drain electrodes, spin coating is used to deposit a two-layer photoresist consisting of LOR3A and S1805 on the silicon substrate (Figure 1.9(B, iii)). Then metal is deposited for the source and drain electrodes by thermal evaporation (Figure 1.9(B, iv)). After removing the remaining photoresist layer by Remover PG, the "bottom-up" processes are finished, as shown in Figure 1.9(B, v).

Compared with the "top-down" method, the "bottom-up" approach has the advantages of synthesizing SiNWs of high crystallinity, designated dopant density, thin silicon oxide sheaths and easily controlled diameters in a cost-effective preparation.

1.6 SiNW sensor design concern – Debye-Hückel screening

In order to keep biomolecules or proteins active in the sensing devices, similar physiological environment as human serum or urine should be created. One common method is to add phosphate buffered saline or phosphate solution in sample solutions during the measurements. However, due to the high-salt concentration in the solution, the variance of electric potential $V(r)$ because of the binding events of receptors on the nanowire surface and biomolecules in the solution would be screened, and thus weakens the detection single obtained from the electrical measurements. If the distance r_{bs} between the binding site and the nanowire surface increases, the screening of electric potential $V(r)$ would be enhanced exponentially, given as

$$V_{screening} = V(r)e^{-r/\lambda_D} \text{ at } r = r_{bs} \tag{1.2}$$

where λ_D is the Debye-Hückel length [81-82] and is given by

$$\lambda_D = \sqrt{\frac{\varepsilon_0 \varepsilon_r k_B T}{2N_A e^2 I}} \tag{1.3}$$

where ε_0 is the permittivity of vacuum, ε_r is the relative permittivity, k_B is the Boltzmann constant, T is the absolute temperature, N_A is Avogadro's number, e is the elementary charge and I is the ionic strength of the electrolytic buffer solution. Calculations from Eq. (1.3) give $\lambda_D = 0.74$ nm for 1 × PBS solution, $\lambda_D = 2.4$ nm for 0.1 × PBS solution and $\lambda_D = 0.74$ nm for 0.01 × PBS solution, which makes sense because the higher ionic strength would lead a shorter Debye-Hückel length.

Figure 1.10 shows the effect of the Debye-Hückel length on the SiNW detection sensitivity. Different ionic concentrations would lead to different Debye-Hückel lengths, and ionic lengths should be carefully controlled to minimize the negative effects of electric screening on the strength of detection signal, as shown in Figure 1.10(A). Lin *et al.* developed a SiNW sensor by functionalizing glutathione (GSH) on the nanowire surface to study the glutahiione and glutathione S-transferase (GST) interactions [83]. Conductance change after introducing 15 nM GST in either 0.1×PBS (black curve) or 1×PS are observed, as shown in Figure 1.10(B). However, after diluting the buffer solution by 10 times, which is either 0.01×PBS or 0.1×PS, the conductance change was enhanced by fourfold, due to the weaker screening effect in diluted solutions, as shown in Figure 1.10(C).

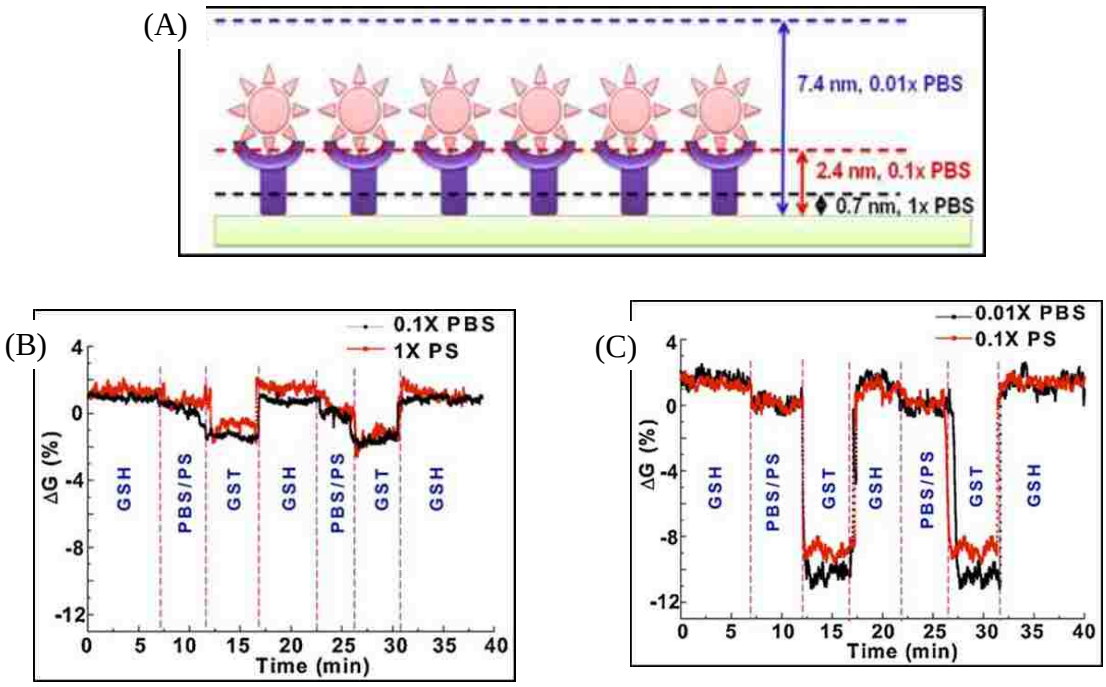

Figure 1.10: (A) Schematic of the height of λ_D from the sensor surface for an electrolytic buffer solution [1]; (B) Real-time electrical measurements in buffer solution 0.1×PBS (black) and 0.1×PS (red) [83]; (C) Real-time electrical measurements in buffer solution 0.01×PBS (black) and 0.01×PS (red) [83].

One method to minimize the screening effects is to judiciously select the subthreshold regime, where the gating effect from target molecules is more effective due to the reduced screening of carriers inside the SiNW [84]. The role of gating effect is strongly affected by the relative magnitude between carrier screening length λ_{Si} and SiNW radius R. In the case with high carrier concentration regime where $\lambda_{Si} << R$, the SiNW biosensor works in a linear regime and the conductance varies with gate voltage linearly. In the low carrier concentration regime $\lambda_{Si} >> R$, the SiNW-FET works in the depletion regime and the conductance varies with gate voltage exponentially. Therefore, the most sensitive SiNW biosensor should have long screening length in the subthreshold regime and the field effect of surface charges can gate the whole SiNW, fully utilizing the

high surface-to-volume ratio of SiNW and effectively reaching the optimal detection sensitivity of the SiNW sensor [1].

Thesis contents

This thesis presents a multiphysics computational model to study the biomolecular detection process with electrokinetic effects. Significant advancements have been achieved in using SiNW sensor to understand biological systems. Specifically, some groups have demonstrated the high sensitivity of SiNW to detect biomolecules in ~10 fM concentration solution within minutes [85-86], which is a great step toward realizing the ultimate goal of biomolecular detection. On the other hand, analytical studies of the diffusive transport of biomolecules toward nanosensor surface suggest that femtomolar concentration detection would require response time as long as a few days [87-88]. In this thesis, various factors that would accelerate the biomolecular detection process are discussed, with a focus on the electrokinetic effects, which are further explored by our multiphysics computational model.

Chapter 2 covers several traditional computational models to predict the performance of SiNW sensors. The most popular model, the "diffusion-reaction theory", which studies the ensemble average of the stochastic behavior of biomolecules, is introduced first, as well as its advantages and limitations. Then, the effect of fluid flow in the microfluidic devices is discussed, in terms of "convection-diffusion-reaction theory". Statistical variance theory based on Monte Carlo method is also presented as a potential reason for the detection time discrepancy. Finally, a computational model based on Brownian dynamics is developed to verify the existence of such time discrepancy and a

discussion about possible factors that account for the three orders' detection time difference at fM concentration is given.

Chapter 3 explores the contributions of electrokinetic effects to the speed acceleration of biomolecular detection process. In the beginning of the chapter, electrokinetic phenomena, including electrophoresis, dielectrophoresis and electroosmosis, are presented in detail, as well as their applications in microfluidic devices. Then, a rigorous mathematical model considering these electrokinetic effects is derived. Multiphysics numerical simulations are conducted to solve this mathematical model, and the trajectories of biomolecules under electrokinetic forces are plotted. Finally, detection time for a typical SiNW sensor with electrokinetic effects is calculated and compared with that based on pure Brownian dynamics.

Chapter 4 provides a deep insight in the various design considerations of SiNW devices with the electrokinetic effects based on the developed computational method. First, an introduction to the previous studies of the design in SiNW sensing devices is presented. Then, the influences of several important factors, including nanowire design, solution gate design and biomolecular charge, on the performance of SiNW sensors, are investigated and discussed in detail. The chapter ends with a discussion about the explanation for the three orders' detection time discrepancy and optimal design for improving the performance of SiNW sensors.

Chapter 2

Computational models for biomolecular detection process

In recent years, the capability of SiNW sensor for detecting biomolecules at ultralow concentration (~ fM) has been demonstrated by various research groups [63, 65, 89]. However, the subsequent theoretical analysis could only partially explain the experimental results, which makes it difficult to establish a framework to guide the further optimization of biosensing devices. These theoretical studies can successfully explain the biomolecular detection process at high concentration (larger than 1 μM), yet do not provide physical insights for the three orders' detection time difference between theoretical predictions and experimental results at ultralow concentration (~ 1 fM). In this chapter, we first briefly review the existing diffusion-reaction theory and its limitations. Secondly, the effect of fluid flow is considered in the diffusion-reaction theory, which is also referred to as "convection-diffusion-reaction theory". Thirdly, the statistical variance theory, which is proposed for explaining the detection time discrepancy, is presented. At the end, a Brownian dynamics model is developed to verify this discrepancy and the potential contributions of other factors to lead the detection time discrepancy at ultralow concentration are discussed.

2.1 Diffusion-reaction theory and its limitations

The simplest sensing system is that the biomolecules diffuse toward the sensor surface in the biological solution and firm binding happens when biomolecules are in contact with conjugate receptors coated in sensing region. Biomolecular diffusion is

characterized by random and stochastic steps without any inter-correlations. The displacement of biomolecules increases as the square root of time, given as [90]:

$$L_D = \sqrt{Dt_s} \tag{2.1}$$

where D is diffusion constant and t_s is the detection or response time. It is obvious that the time for a biomolecule to reach the biosensor surface would scale as the square of the diffusion distance, given as:

$$t_s \sim \frac{L_D^2}{2D} \tag{2.2}$$

Based on the above two equations, one can track each biomolecule, and thus obtain the response time of biosensors to collect enough biomolecules to trigger a signal. However, this is a challenging work, especially for the case with high analyte concentration. For example, if the concentration of biomolecules is 1 nM, then there would be 10^6 biomolecules in a volume of 1000 μm^3. Tracking the movements of all these biomolecules would be computationally expensive.

In order to reduce the computational cost, the diffusion-reaction theory is proposed to describe the movement of biomolecules in solution. In this theory, an ensemble average of the stochastic behavior of individual biomolecules is introduced in terms of concentration field c. This ensemble average could be obtained by averaging many single-molecule experiments or simulations and is naturally reproduced by concentrated solutions, where a great number of biomolecules act simultaneously within the relevant experimental window. In the extremely diluted solution, where the concentration would be as low as 1 fM (1 biomolecule in 1000 μm^3), the concentration profile would appear granular in the solution. However, averaging the results of many such experiments or

simulations would lead to a smoothly varying concentration profile [91], as described below.

Table 2.1: Expressions for the dimension dependent parameters used in Eqs. (2.3) ~ (2.10) [88].

	M_D	k_D	A_D	$C_{D,SS}$	$C_{D(t)}$
Planar ISFET	$\frac{1}{2}$	$N_s\sqrt{\frac{2}{D}}$	1	$\frac{D}{W}$	$\frac{D}{\sqrt{2Dt}}$
Cylindrical nanowire	1	$\frac{N_s a_0}{D}$	$2\pi a_0$	$\frac{2\pi D}{\log[(W+a_0)/a_0]}$	$\frac{2\pi D}{\log[(\sqrt{4Dt}+a_0)/a_0]}$
Nanosphere	1	$\frac{N_s a_0}{D}$	$4\pi a_0^2$	$\frac{4\pi D}{a_0^{-1}-(W+a_0)^{-1}}$	$\frac{4\pi D}{a_0^{-1}-(\sqrt{6Dt}+a_0)^{-1}}$

Consider an isolated sensor immersed in a static analytic solution, the conservation equation for analyte concentration can be described as:

$$\frac{\partial c}{\partial t} = D\nabla^2 c \tag{2.3}$$

The sensor surface is functionalized with specific receptors, and once target biomolecules move close to these receptors, the binding process would begin to take effect, given as:

$$\frac{\partial N}{\partial t} = k_{on}\left(N_0 - N\right)c_S - k_{off}N \tag{2.4}$$

where k_{on} and k_{off} are the binding and disassociation constants, N is the surface concentration of bound analyte, c_S is the analyte concentration at the surface boundary, and N_0 is the density of binding sites on the sensor. The particle flux at the sensor surface is given by

$$I = D\int_{A_D} \nabla_n c ds \tag{2.5}$$

where I is the integrated incident flux to the sensor and A_D is the dimension-dependent areas of the sensor surface, as shown in Table 2.1. By solving Eqs. (2.3) (2.4) and (2.5) simultaneously, the relationship among various sensor parameters, such as the response time of biosensors, could be obtained. By assuming a large k_{on}/k_{off} (~ 10^5 for specific target receptor combinations [92]), and N_0 (~10^4 μm^{-2} [93]), Eq. (2.4) could be simplified as

$$\frac{dN}{dt} \sim k_{on} N_0 c_S \tag{2.6}$$

Then an excellent approximation to exact solution of Eq. (2.3) can be derived by generalizing the approach by Berg [90], and the solution in any dimension at steady state is given as

$$I = JA_D = C_{D,SS}\left(c_0 - c_S\right) \tag{2.7}$$

where $C_{D,SS}$ is the diffusion equivalent capacitance, as shown in Table 2.1, and c_0 is the equilibrium analyte concentration at a distance W from the sensor surface. Due to the balance between the incident flux and the conjugation flux that $J = dN/dt$, the steady state flux to the sensor surface could be calculated by solving Eq. (2.6) and (2.7), given as

$$N\left(t\right) = c_0 t\left(\frac{A_D}{C_{D,SS}} + \frac{1}{k_{on}N_0}\right)^{-1} \tag{2.8}$$

Instead of fixing the depletion distance W, we set $W = \sqrt{2nDt}$, where n is the dimensionality of the sensor and n is 1, 2, 3 for planar sensor (1D), nanowire sensor (2D) and nanosphere sensor (3D), respectively. Therefore, the transient response of the sensor could be obtained as

$$N(t) = c_0 t\left(\frac{A_D}{C_D(t)} + \frac{1}{k_{on}N_0}\right)^{-1} \tag{2.9}$$

where $C_D(t)$ is a newly defined diffusion equivalent capacitance as a function of $W(t)$. Assume the response time t_s to be the time required to capture N_s biomolecules and $k_{on} \to \infty$, Eq. (2.9) together with the relations given in Table 2.1 leads to the following scaling relationship [88], given as

$$c_0 t_s^{M_D} \sim k_D \tag{2.10}$$

where M_D and k_D are sensor-dimensionality dependent constants, as shown in Table 2.1.

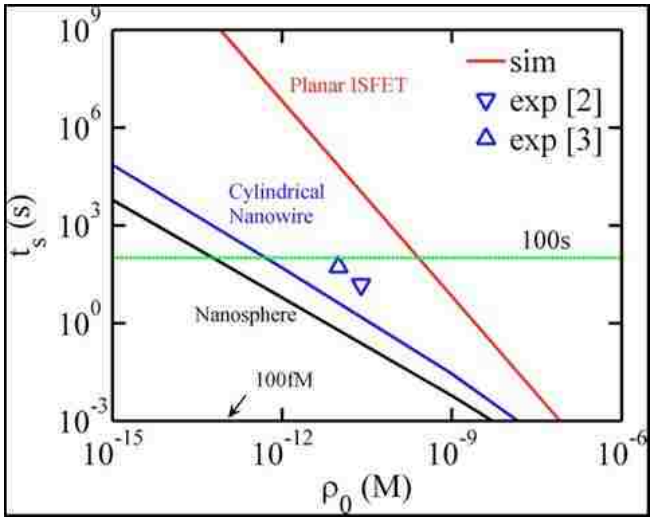

Figure 2.1: Response time of various nanosensors over different concentrations [88].

Based on the Eq. (2.10), a number of conclusions could be made. Figure 2.1 shows the response time at different concentrations for a typical DNA detection problem using three different types of biosensors: planar sensor (1D), cylindrical nanowire sensor (2D), and spherical sensor (3D). Firstly, the response time for nanowire sensor is far more less than planar sensor at the same analyte concentration, but the difference between response

time of nanowire sensor and spherical sensor is negligible, which indicates the importance of development of nanowire sensor and nanosphere sensor. Secondly, femtomolar detection using nanowire sensor would take several hours to days, which means it is challenging for nanowire sensor to achieve ultrafast detection at ultralow concentration. Nair *et al.* claimed that reducing the diameter of the sensor, decreasing the minimum number of analytes required for detectable signals and increasing the effective diffusion coefficient by increasing the ambient solution temperature would lead to a reduction of response time [88]. At high analyte concentration, these conclusions work well and could provide some physical sense about biosensing detection process. However, experiments with SiNW sensors show a clear signal within seconds to minutes, instead of several hours or days, after 10 fM target concentration is introduced [85-86], which indicates some other factors may play an important role in enhancing the transport of biomolecules toward SiNW surfaces.

2.2 Convection-diffusion-reaction theory and its limitations

The diffusion-reaction theory is based on purely diffusion of biomolecules. However, in a typical microfluidic device, the solution is not always static but moves across the sensor surface with a certain velocity. Therefore, some researchers proposed that the convective transport of biomolecules due to fluid flow would account for the gap of detection time between theoretical calculations and experimental measurements [87, 91]. In the following part, the effect of fluid flow on the biomolecular detection process is explored.

After considering the effect of fluid flow on the transport of biomolecules, the conservation equation for analyte concentration would be changed to:

$$\frac{\partial c}{\partial t} = D\nabla^2 c - \mathbf{u}\cdot\nabla c \tag{2.11}$$

where $\mathbf{u}$ is the velocity of surrounding flow. Solving Eqs. (2.4) (2.5) and (2.11) simultaneously, then exact solutions of parameters in the biosensing process could be obtained. However, the simple addition of the velocity complicates the mathematical solution tremendously, and thus numerical simulations are performed to solve the phenomenon about biomolecular transport with fluid flow.

Before going to the details of numerical simulation results, one important parameter "Peclet number" should be introduced. The Peclet number is a dimensionless number relevant in the study of transport phenomena in fluid flow and is defined as the ratio of the rate of advection of a physical quantity by the flow to the rate of diffusion of the same quantity driven by an appropriate gradient [94-95], given as

$$Pe = \frac{\text{diffusion time}}{\text{convection time}} = \frac{L^2/D}{L/v} = \frac{vL}{D} \tag{2.12}$$

where L is the travelling distance and v is the velocity of fluid flow. When $Pe << 1$, the transport of biomolecules is mainly due to Brownian diffusion. On the other hand, when $Pe >> 1$, the fluid flow helps the transport of biomolecules significantly.

Figure 2.2 illustrates the effect of fluid flow on biomolecular detection process numerically. The model considered here is a two-dimensional channel, and the sensing region is a narrow planar area in the middle of the channel. The fluid flow in the channel is filled with target biomolecules and it is assumed that biomolecules bind with the sensor

surface firmly ($k_{on} \to \infty$) when they are in contact with each other. In the case of purely diffusive transport, a depletion zone forms due to the collection of target biomolecules on the sensor surface. This depletion zone starts relative flat, until its thickness becomes comparable to the sensor size. Then it goes radically until it spans the channel, after which it extends into the channels and grows indefinitely, as shown in Figure 2.2(A, i). One thing that should be mentioned here is that the steady state is never reached in this system. In addition, the depletion zone grows ever larger, diffusive flux gets even smaller, and collection even slower [91].

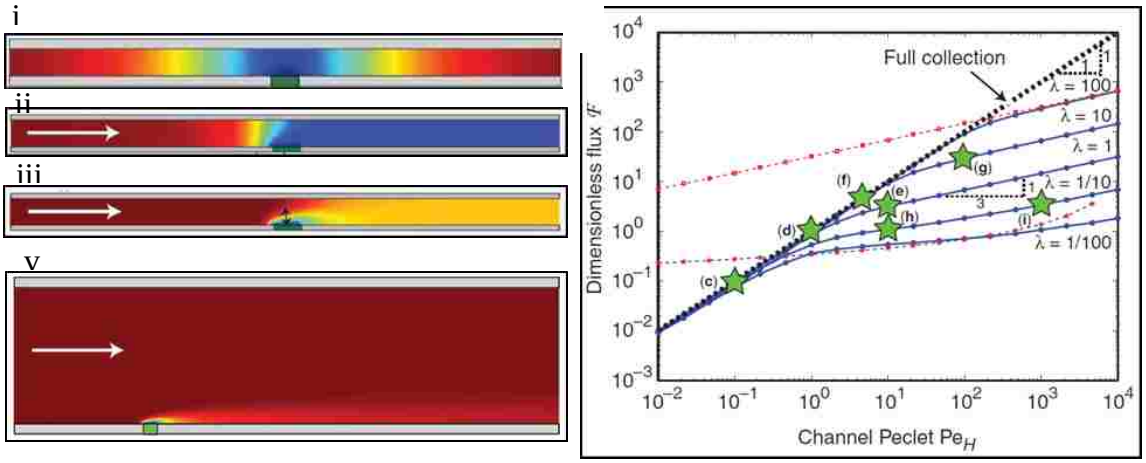

(A) (B)

Figure 2.2: (A) Steady concentration profiles under different values of Pe. (B) Steady-state flux to the sensor surface under both convection and diffusion. [91]

Consider an extremely slow flow rate is introduced into the channel, in this case $Pe << 1$. The convection flow halts the indefinite growth of depletion zone in the purely diffusion simulation and gives a steady depletion zone with just the right length for the target flux delivered by convection to balance the diffusive flux, as shown in Figure 2.2(A, ii). If the diffusive flux is larger than the convective flux at the interface, then the depletion zone would grow and expand. In contrast, in the case that the diffusive flux is

smaller than the convective flux, the depletion zone would be compressed. For slow enough flow rates, the sensor could collect every injected target biomolecule [91].

As we increase the flow rate, the steady concentration profiles change substantially, as illustrated in Figure 2.2(A). In the case of extremely fast flows ($Pe >> 1$), many biomolecules would be flowed downstream before they can diffuse very far and the biomolecules in a thin layer have chance to be collected by the sensor (Figure 2.2(A, v)). The flux through the depletion zone can be estimated as [96]

$$J\left(Pe >> 1\right) \sim 0.81Pe^{1/3} + 0.71Pe^{-1/6} - 0.2Pe^{-1/3} \cdots \tag{2.13}$$

Based on Eq. (2.13), even though the flow rate is increased by 1000 times, the flux on the sensor surface would only be enhanced by 10 times. This weak relationship between flow and flux is insufficient to explain the three orders of magnitude of detection time discrepancy between measured values and the mass-transport limits for nanosensors. There must exist some other factors that accelerate the speed of biomolecular detection process.

2.3 Statistical variance theory and its limitations

There are large stochastic variances associated with biomolecular detection, but the influence of such statistical variance on biomolecular sensing process is not captured by the diffusion-reaction theory or convection-diffusion-reaction theory. Go *et al.* claimed that the persistent gap between reports of analyte detection at approximately femtomolar concentration and theoretical predictions is due to the statistical variations. The predicted theoretical detection time based on diffusion-reaction theory is actually relevant for practical nanosensors only in the sense of an ensemble average time when 50% of the

sensors in a large sensor array register the existence of target biomolecules. However, in reality, the biosensor would present a signal if 5 ~ 10% of the sensors could detect the presence of target biomolecules. The discrepancy of detection time maybe would be explained by the time difference of the mean response time and the minimum response time [97].

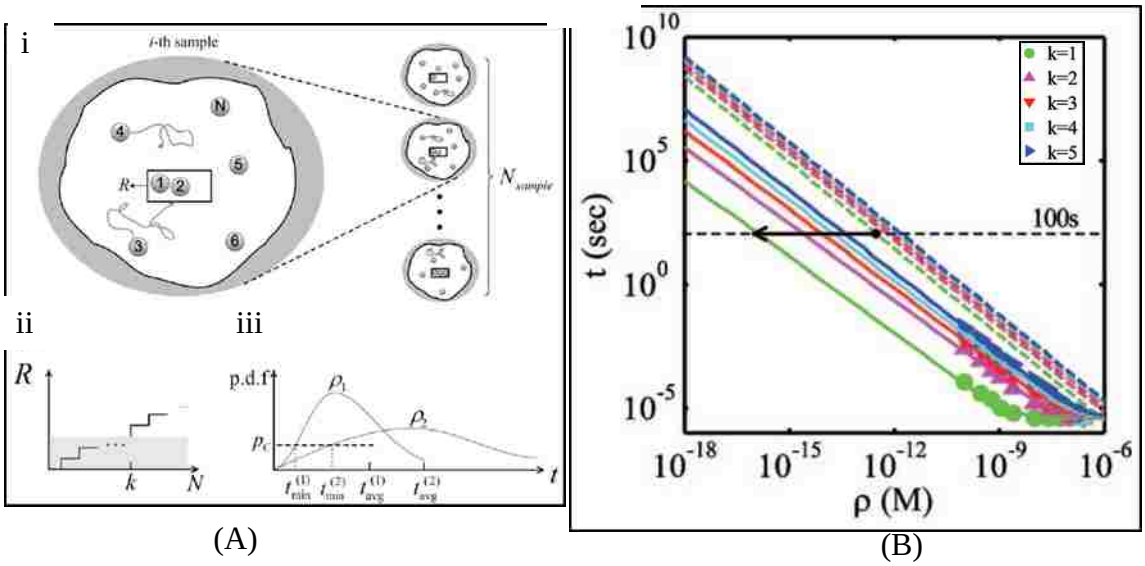

Figure 2.3: (A) Schematic of an ensemble of NW-based biosensors and detection mechanism considering statistical variances; (B) The minimum and average detection time of the k_{th} biomolecule. [97]

Figure 2.3(A, i) shows a schematic of an ensemble of a biosensing system, which is assembled by N nanowire-based sensors. Each nanosensor needs to have enough binding events happening on the sensor surface to trigger a signal. For example, a detection signal could be generated once a minimum of k biomolecules are captured. If the number of binding events is less than k, then the signal would be suppressed by the surrounding electrical noise, as shown in Figure 2.3(A, ii). The detection time differences between average detection time and minimum detection time at different concentrations

are plotted in Figure 2.3(A, iii). At high concentration, the difference between average and minimum detection time is small, whereas the gap becomes larger as the concentration decreases, which indicates that the statistical variance may be the reason that leads to many orders' detection time difference at ultralow concentration.

In order to explore the effect of statistical variances on the biomolecular detection time, Go conducted numerical simulations using a variant of the Monte Carlo (MC) method – the so-called "table-based MC (TMC) approach" [98]. The basic idea of TMC is to use the MC method to numerically calculate and tabulate the capture time distributions for biomolecules injected at various starting positions to numerically precalculate and store the Green's function [99] from any random starting point to the sensor surface. For example, the $(i, j)_{th}$ element of the table, $G_{i,j} \equiv G(r_i, t_j)$ describes the probability that a biomolecule injected at location r_i at time $t = 0$ is captured by the sensor at time $t_j = j\Delta t$. For calculation proper, a sample S is first created by specifying the initial position of the biomolecules $(r_k^S; k = 1,..., M)$ consistent with a specific density of analyte c_M. For each particle from r_k^S, its capture time by the sensor is stochastically chosen to be consistent with the precalculated arrival-time distribution from that point, $G_{i,(.)} \equiv G(r_i...)$. The process is repeated for all M analyte biomolecules of the sample S to obtain a sorted list of arrival times, $t_{s,m}; m = 1...M$. If k is the number of particles required for an observable sensor response, then $t_{s,m=k}$ is the initial response time for this

sensor. The process is repeated for large number of samples $\left(N \sim 1000\ s\right)$ to establish an k_{th} arrival-time distribution at a particular density of analytes $\left\{t_{s=1...N;k}\right\}$ [97].

As an illustrative example, an ensemble of 2000 NW-based biosensors $N = 2000$ is studied. The average detection time is assumed to be the time when ~50% of sensors indicate the presence of target biomolecules, and the minimum detection time is set to be the time when 1% of the sensors trigger a detection signal [97]. Figure 2.3(B) shows the minimum detection time and average detection time as a function of concentration. In the case that one biomolecule is enough to trigger the detection signal for each sensor, the average detection time is three orders of magnitude larger than the minimum detection time, which provides a simple resolution of the gap between previous theoretical results and experimental demonstrations. In addition, the detection time difference becomes smaller and vanishes at high concentration, which could explain why such an issue is not obvious for biosensing at high concentration. However, experiments on a single nanosensor have consistently observed fM detection within a few minutes, thus indicates that factors, other than flow rate and statistical variance, should be taken into account for resolving the puzzle about the biosensing process at femtomolar concentration.

Electrokinetic effects, which are mainly due to the applied voltage on the solution gate, are considered and investigated for their contributions to the acceleration of biomolecular detection process through a multiphysics computational model. In order to demonstrate of the accuracy of our computational model for describing the biomolecular sensing problem, a benchmark based on Brownian dynamics is studied, as described below.

2.4 Brownian dynamics modeling of biomolecular detection process

Using Brownian dynamics to model detection process has two advantages over traditional diffusion-reaction models: First, at ultralow concentration such as fM, there is only one molecule in a volume of 1000 μm^3, thus assumptions for diffusion-reaction theory are not valid anymore and a Brownian dynamics model is more appropriate. Second, due to its stochastic nature, a Brownian dynamics model is very similar to the real detection process, which is dominated by random initial positions of the molecules as well as the random diffusion/binding process. Therefore, a benchmark based on Brownian dynamics is used to evaluate the accuracy of the developed computational model in analyzing biomolecular detection process.

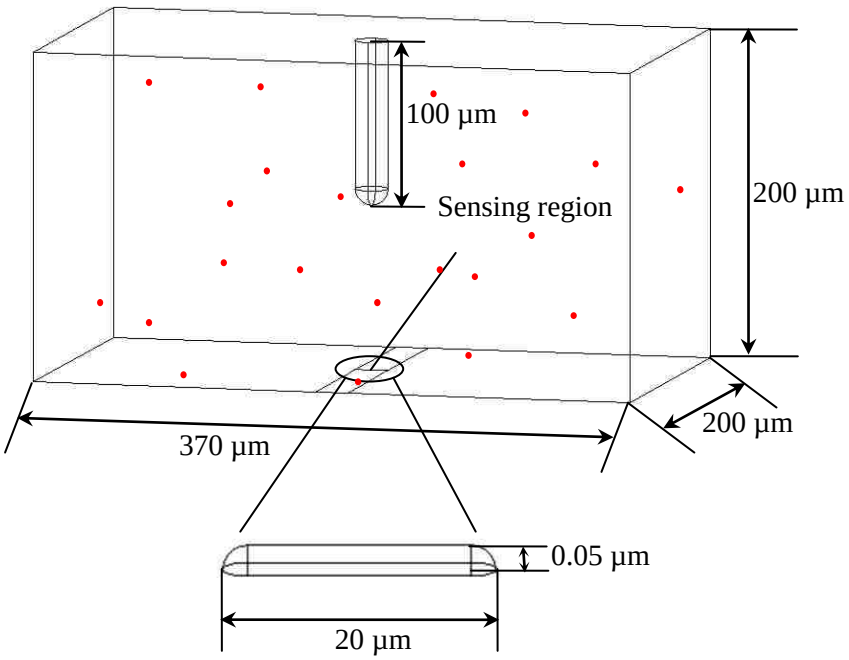

Figure 2.4: A Brownian dynamics model for SiNW sensors, with randomly distributed biomolecules (red dots) in the fluid domain.

The Brownian dynamics model developed for a typical SiNW sensor is created using COMSOL Multiphysics®, as shown in Figure 2.4. Randomly distributed biomolecules move with the fluid flow through a channel of height 200 µm and width 370 µm. A finite length of channel 200 µm is adapted to simplify the simulation. The SiNW is treated as a semi-cylinder of diameter 100 nm and length 20 µm on the bottom surface of the model and the solution gate is modeled as a cylinder of length 100 µm and radius 10 µm attached to the top wall. The electrokinetic effects due to the gate voltage are studied by solving Navier-Stokes equations and Gauss's law simultaneously, and results of multiphysics modeling of SiNW sensors are presented in detail in Chapter 3.

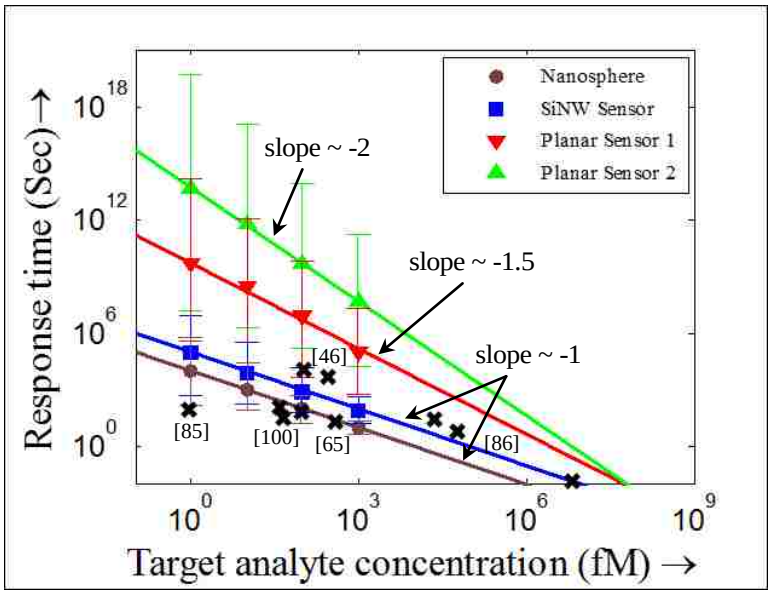

Figure 2.5: Response time of various nanosensors at different concentrations. Error bars are plotted to show the statistical variances of numerical calculations. Experimental reported values are also shown as black crosses.

In the above Brownian dynamics model, biomolecules of different concentrations are injected into the fluid domain as the initial configuration. For example, 90 biomolecules are randomly distributed in the fluid domain at an analyte concentration 10 fM. The diameter of biomolecules is assumed to be 10 nm with a diffusion coefficient

4.3654×10^{-11} m^2/s. The movement of biomolecules is dominated by Brownian motion and interactions among biomolecules are ignored. The nanowire is surrounded by a static analyte solution, and firm binding happens as biomolecules are in contact with the nanowire surface, which means the biosensing process considered here is a diffusion-limited problem with binding constant $k_{on} \to \infty$. Furthermore, three binding events are assumed to be enough to trigger a detectable signal, and the arrival time for the third biomolecule is treated as the response time for the SiNW sensor. All the simulations are repeated 10 times, and the average of response time for these 10 trails is treated as the detection time of SiNW sensor at that concentration.

Figure 2.5 shows the results obtained from Brownian dynamics simulations of biomolecular detection process. The detection time for biomolecular concentration from 1 fM to 1 pM is calculated. Four different types of sensors, a nanosphere sensor of diameter 1 μm, a SiNW sensor of diameter 100 nm and length 20 μm, a planar sensor of width 20 μm and length 200 μm, a planar sensor of width 370 μm and length 200 μm, are investigated. The response time decreases dramatically with the increase of biomolecular concentration, with a slope of around -1, -1, -1.5, -2 in logarithm for nanosphere, nanowire, and planar sensors, respectively. This is consistent with theoretical prediction from diffusion-reaction theory [88]. Specifically, at analyte concentration 1 fM, the response time for planar sensor is two hundred times as large as that of SiNW sensor, which indicates the huge advantage of SiNW sensor in biomolecular detection at ultralow concentration. In addition, as illustrated in Figure 2.5, it would need more than one day for a typical SiNW sensor to detect target biomolecules at concentration 1 fM, which is

far beyond the time limits in clinical diagnosis and lab experiments. However, experimental results [46, 65, 85-86, 100], plotted as black crosses in Figure 2.5, imply that nanosensors could always present a clear signal of detection process at fM concentration in several minutes, which means a three-order magnitude of detection time gap between theoretical predictions and experimental results.

As described at the beginning of this section, Brownian dynamics simulations have the advantage of capturing the statistical variances, compared with the diffusion-reaction modeling. The statistical variances are plotted as error bars in Figure 2.5. The length of error bars is proportional to the magnitude of the variances in logarithm. As the analyte concentration increases, the statistical variance reduces. In other words, the more sensitive the biosensor is, the larger the response time variance. This is because while the binding of individual biomolecule is random, the collective binding results of a large number of biomolecules are determinant. However, the variance in response time for a single SiNW sensor is limited (STD < 0.25). Such small statistical variances can't give satisfactory descriptions of the biosensing process at ultralow concentration.

So far, two factors, flow rate and statistical variance, have been investigated in the biomolecular detection process, but couldn't give a reasonable explanation for detection time discrepancy at ultralow concentration. Other factors that may enhance the transport of biomolecules toward the SiNW surfaces include electric field, magnetic field and so on. Particularly, electric forces, with tunable amplitude and easy experimental setup, have been successfully applied to manipulate different biomolecules and cells. However, there has not been a study about how electric forces change the biomolecular binding process

in SiNW sensors. In the next chapter, we would apply the developed multiphysics model to characterize the effects of electric field on biomolecular detection speed.

Chapter 3

Electrokinetic effects on biomolecular detection process

Due to the existence of solution gate voltage, biomolecules in the SiNW devices would be subject to electrokinetic effects, such as electrophoretic force, dielectrophoretic force, electroosmotic flow, and electrothermal effect. These electrokinetic effects would change the behaviors of biomolecules, and thus could possibly enhance the transport of biomolecules toward SiNW surfaces and lead to a significant reduction of response time. In this chapter, some major electrokinetic phenomena, including electrophoresis, dielectrophoresis and electroosmosis, are presented in detail. Then a rigorous mathematical model for biomolecular detection process with electrokinetic effects is developed. The corresponding governing equations are solved by our developed multiphysics computational model. The trajectories of biomolecules under electrokinetic effects are plotted and detection time at different concentrations is recorded and discussed at the end of the chapter.

3.1 Electrokinetic phenomena in microfluidics

The controlled manipulation of biomolecules and cells is drawing more and more attention in transport, alignment, and assembly of nano- and bio-materials in microsystems, such as fuel cells, medical devices and biological or chemical sensors [101-102]. The major challenge for the manipulation lies in the small length scale of nano and bio-materials, which limits the effective observation. Various mechanisms, such as fluid flow, electrokinetic effects, magnetic field and acoustic field, have been proposed in

recent years to control the movement of biomolecules and cells. Among them, electric forces, with tunable amplitude and easy experimental setup, have been successfully applied to manipulate different biomolecules and cells [103]. An applied electric field would introduce several major effects such as electrophoresis, dielectrophoresis, and electroosmosis, as described below.

3.1.1. Electrophoresis and its applications

Generally, most surfaces would acquire electric charge due to ionization, ion adsorption or ion dissolution, when they are in contact with an aqueous medium [104]. The surface charge, in turn, would influence the distribution of nearby ions in the solution by attracting ions of opposite charge toward the surface. Ions of like charge would be repelled away from the surface. This electrostatic interaction together with the mixing tendency resulted from the random thermal motion of ions, leads to formation of an electric double layer (EDL), as shown in Figure 3.1(A). The electric double layer consists of two parts, a compact layer and a diffuse layer. The electric double layer is a region close to the charged surface in which there is an excessive of counter-ions over co-ions to neutralize the surface charge. Evidently, there is no charge neutrality within the double layer because the number of counter-ions is greater than the number of co-ions. Upon application of a tangential external electric field, the interaction between the net charge in the EDL and the electric field would cause the relative motion of either the liquid or the solid phase [102].

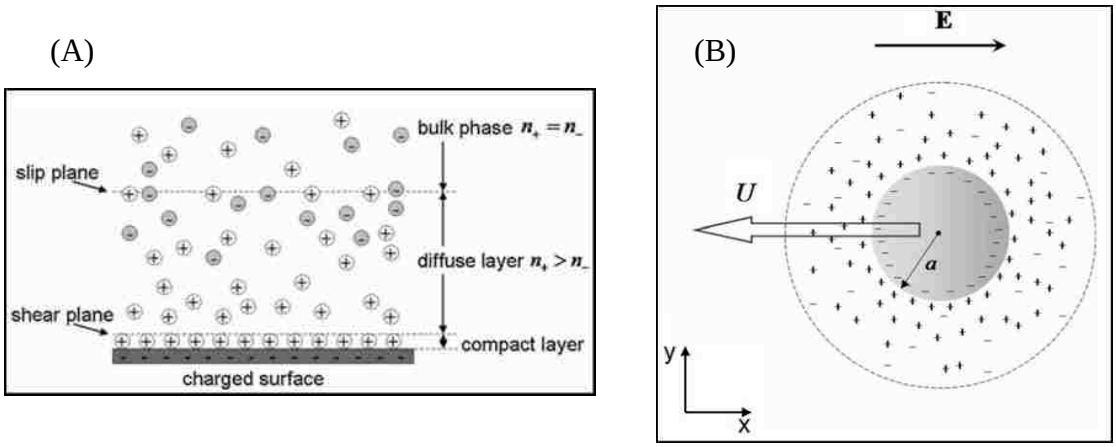

Figure 3.1: (A) Schematic of the electric double layer (EDL) structure; (B) Schematic of the electrophoretic motion of a spherical particle. The thickness of the double layer to the size of the particle is not drawn to scale. [102]

For a system including a particle and a continuous suspending polar medium, an EDL is formed near the surface of the particle, as shown in Figure 3.1(B). A negatively charged particle is surrounded by a diffusive layer which contains excessive number of positive mobile ions. The charged particle moves toward the electrode of opposite electrical polarity under the uniform or homogeneous external electric field. This movement is due to the Coulombic force, generated by the interaction between the net charge on the particle and the applied electric field. The electrophoretic force acting on a particle with a net charge q under electric field strength $\mathbf{E}$ is given by

$$\mathbf{F}_{EP} = q\mathbf{E} \tag{3.1}$$

The electrophoretic velocity with which the particle moves with respect to its suspending medium is proportional to the applied electric field strength by a factor called electrophoretic mobility. The electrophoretic mobility μ_{EP} is proportional to the magnitude of the net charge on the particle, and is inversely proportional to the size of the particle [104]

$$\mu_{EP} = \frac{\mathbf{U}_{EP}}{\mathbf{E}} = \frac{q}{f} \tag{3.2}$$

where $\mathbf{U}_{EP}$ is the electrophoretic velocity, $f = 6\pi\mu a$ is the Stokes frictional factor for a spherical particle in a creeping flow, μ is the viscosity of the suspending medium and a is the radius of the spherical particle.

Most studies using on-chip electrophoretic force focus on separation or characterization of biomolecules, such as viruses, proteins and DNA. For instance, Reichmuth *et al.* developed novel microchip-based electrophoretic immunoassays using an integrated nanoporous membrane for sensitive and rapid detection of swine influenza virus, as shown in Figure 3.2 [105]. Initially, some virus sample is loaded in the sample (S) well. Then, the sample is transported into the offset T injector toward the sample waste (SW) well and concentrates on the polyacrylamide element using an applied potential of 400 V at the SW well for 120 s while grounding the S well. In order to remove the excess virus sample through the membrane, waste well (W) is put to 800 V for 4 min and SW is grounded. This new assay detects inactivated swine influenza at a concentration four times lower than the traditional open-channel electrophoresis assay and thus provides a sensitive platform for the rapid and portable detection of viruses for livestock screening applications. Huang *et al.* described a micro-scale device, composed of an array of micro-scale posts and integrated microfluidic channels, to sort large DNA fragments using electrophoresis [106]. The electrophoresis is generated by asymmetric pulsed electric field operating alternately at two different angles. For longer DNA polymers, it would take more time slithering back and forth in the channel defined by the posts over which it is draped, with less time moving in the direction of the average field.

The mixed DNA polymers would eventually be separated into different bands, the angles of which depend on their polymer lengths. This method could sort large DNA fragments (61-209 kilobases (kb)) in 15 seconds with a resolution of ~13%, which is substantially advantageous over other techniques.

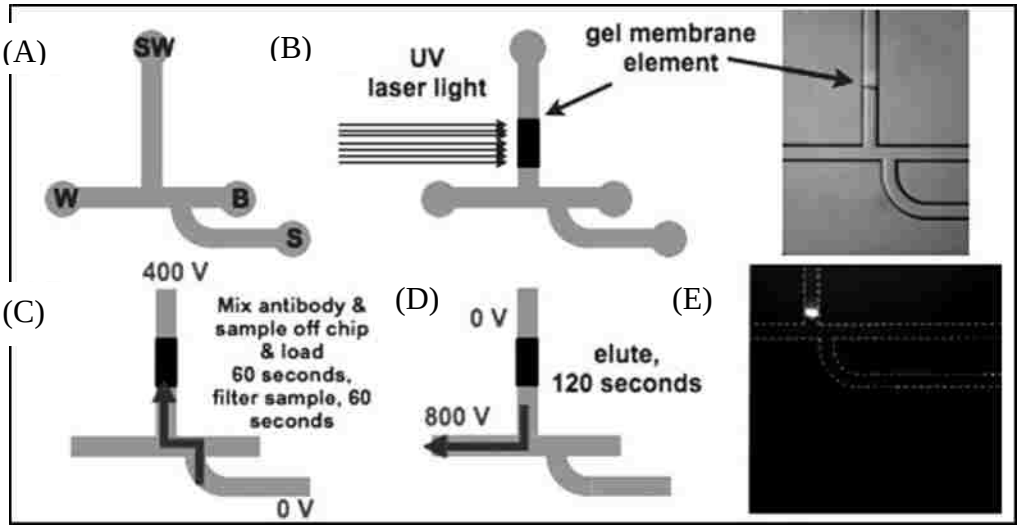

Figure 3.2: (A) Schematic of the microfluidic chip. S, SW, B and W are sample, sample waste, buffer and waste, respectively; (B) Formation of a 6% polyacrylamide plug using UV laser; (C) Concentrate virus and antibody in the plug region using electrophoresis; (D) Remove excess virus and antibody using electrophoresis; (E) Detect viral particles using epifluoresence microscopy. [105]

Another important application of electrophoresis is to manipulate living cells. Toriello *et al.* developed a microfluidic cell capture system using inter-digitated gold electrodes microfabricated on a glass substrate within PDMS channels [107]. The cell surface is labeled with thiol functional groups using endogenous receptors to the cell adhesion peptide sequence RGD. The labeled cells are electrophoretically directed to selected gold electrodes, due to their intrinsic negative surface charge. Maximum single-cell capture is attained for the 10-min trial, with 63 ± 9% (n=30) of the electrode pad rows having a single cell. This device provides a novel platform for future single-cell

genetic studies. Ozkan *et al.* presented an electro-optical system for the rapid parallel arraying and subsequent serial manipulation of living mammalian cells [108]. The manipulation of cells is based on two active methods. One is the electrophoretic arraying of cells in a DC field due to their intrinsic negative surface charge. The other is the remote optical manipulation of individual cells by vertical-cavity surface emitting laser driven infrared optical tweezers. The performance of the device is tested using polystyrene beads, as shown in Figure 3.3(A) and (B). Then, the neural progenitor cells are injected into the device and exhibit a random distribution at beginning. After applying a bias of 2 V for 10 min, the progenitor cells assemble into an organized array, as shown in Figure 3.3(C). This approach complements the existing repertoire of both passive and active techniques for cellular arraying on surface and may enable parallel interrogation of cell populations for cell-based assays in drug development and functional genomics.

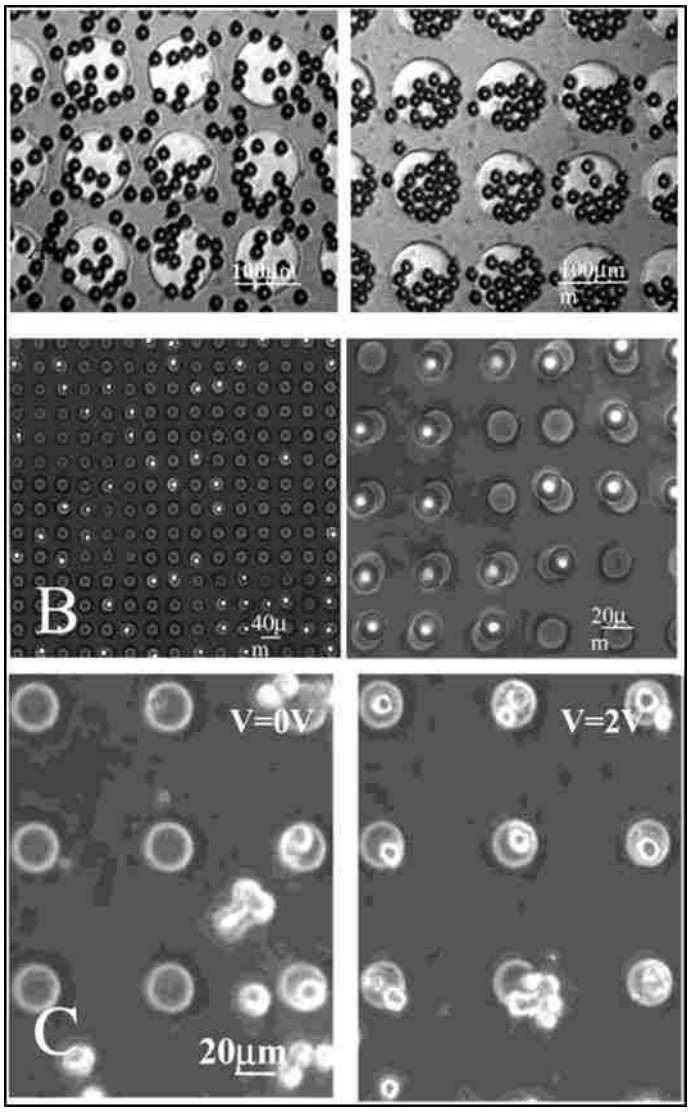

Figure 3.3: Electrophoretic assembly of polystyrene beads and neutral stem cells: (A) Assembly of 20 µm polystyrene beads on silicon/silicon nitride electrode array; (B) Assembly of single 20 µm bead on a 25 µm diameter agarose-patterned ITO electrode array; (C) Assembly of live neural progenitor cells on a 25 µm diameter agarose-patterned ITO electrode array. [108]

3.1.2. Dielectrophoresis and its applications

Dielectrophoretic force arises from the interaction between a dielectric particle in a dielectric suspending medium and a non-uniform electric field. As shown in Figure 3.4, a dielectric particle and the suspending medium become polarized when they are subjected

to an electric field [102]. Because of the polarization, electric charge separation occurs within the dielectric particle as well as in the liquid side of the solid-liquid interface, giving rise to a dipole moment. The effective dipole moment of a spherical particle is given as [103, 109]:

$$\mathbf{p}_{eff} = 4\pi\varepsilon_m a^3 \cdot \mathbf{K}_{CM}\left(\varepsilon, \sigma, w\right) \cdot \mathbf{E} \tag{3.3}$$

where $\mathbf{K}_{CM}\left(\varepsilon, \sigma, w\right)$ is the Clausius-Mossotti (CM) factor, which is dependent on the dielectric properties of the particle and the suspending medium, as well as the frequency of the external electric field. CM factor is a measure of the effective polarizability of the particle in the medium and is given by

$$\mathbf{K}_{CM} = \frac{\varepsilon_p^* - \varepsilon_m^*}{\varepsilon_p^* + 2\varepsilon_m^*} \tag{3.4}$$

where $\varepsilon_{p,m}^*$ are the complex permittivities of the particle and medium, respectively. For homogeneous particle and medium, the complex dielectric constant is given by

$$\varepsilon_{p,m}^* = \varepsilon_{p,m} + \frac{\sigma_{p,m}}{jw} \tag{3.5}$$

Different from the electrophoretic force that is the Coulombic force acting on the net charge of the particle, the dielectrophoretic force is actually the net of the unbalanced Coulombic force acting on the induced dipole. In terms of the dipole moment, the DEP force is given as

$$\mathbf{F}_{DEP} = \mathbf{p}_{eff} \cdot \nabla \mathbf{E} = 2\pi\varepsilon_m a^3 \cdot \mathrm{K}_{CM}\left(\varepsilon, \sigma, w\right) \cdot \nabla \left|\mathbf{E}\right|^2 \tag{3.6}$$

Eq. (3.6) implies that the strength of the DEP force depends strongly on dielectric properties of the medium and the particle, particle's shape and size, as well as the

frequency, amplitude, and the non-uniformity of the electric field. However, this force does not require the particle to be electrically charged. As long as there is an induced dipole moment, all of the particles exhibit DEP in the presence of a non-uniform electric field [102].

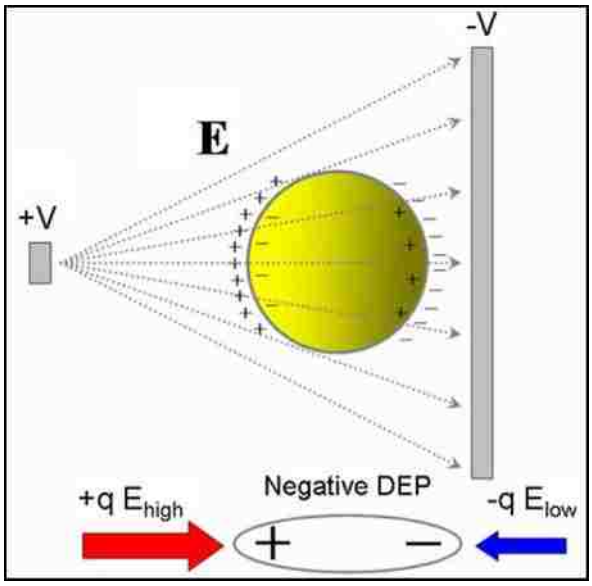

Figure 3.4: Schematic illustration of the negative dielectrophoretic motion of a spherical particle [102].

In most of the cases, the non-uniform electric field for DEP is generated by AC electric field, and the modulation of DEP force is based on the change of driving frequency of the electric field. Over the whole spectrum of driving frequency, different type of cells or particles exhibit distinct response profile range from positive DEP to negative DEP, which has been extensively applied in cell/particle separation, positioning or patterning, focusing and other applications.

Separation of particles or cells using DEP is often achieved by slim and planar interdigitated electrode arrays, as shown in Figure 3.5. A set of electrodes in the sidewall of the microchannels is used for the generation of non-uniform electric fields to generate

DEP forces that repel beads/cells from the side walls. A countering DEP force is generated from another set of electrodes patterned on the opposing sidewall. These lateral negative DEP forces can be adjusted by the voltage and frequency applied. By manipulating the coupled DEP forces, the particles flowing through the microchannel can be positioned at different equilibrium points along the width direction and continue to flow into different outlet channels [110]. In addition, DEP force could be flexibly combined with other techniques, such as gravity, laser and electrowetting for creating separation microdevices of high performance [111-112].

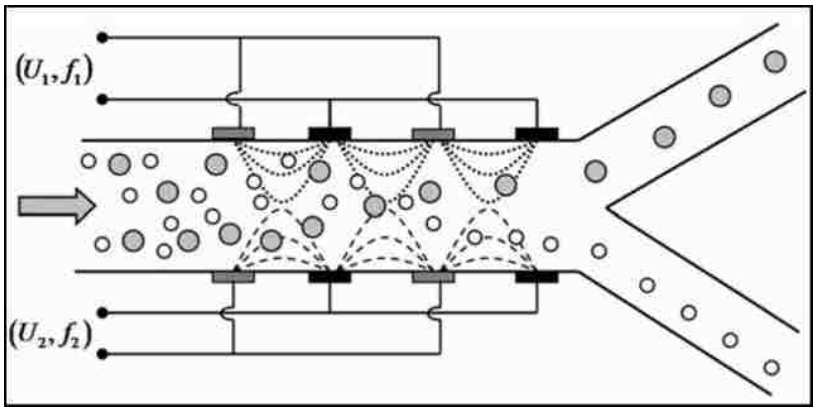

Figure 3.5: Schematic of dielectrophoretic field flow fractionation [110].

Other than the batch manipulations such as separation, DEP could also be used to isolate and identify certain rare cells or particles in clinical sample. Li *et al.* presented DEP tweezers to characterize the interaction between a particle and a surface [113]. Negative DEP force is used to remove a particle from a surface and the force needed to remove the particle can correlate to the strength of the interaction between the particle and the surface. Borgatti *et al.* designed a microdevice for programmable binding of microspheres to target cells for applications of drug delivery and diagnosis [114]. They constructed DEP cages in which the microspheres were forced to bind with single tumor

cells. Figure 3.6 shows a DEP cage for capturing a single yeast cell. Cells are reported to be successfully cultivated over several hours while suspended contact-freely in cell medium by negative DEP force. This method could be used to optimize the physiological conditions for cultivating cells [115].

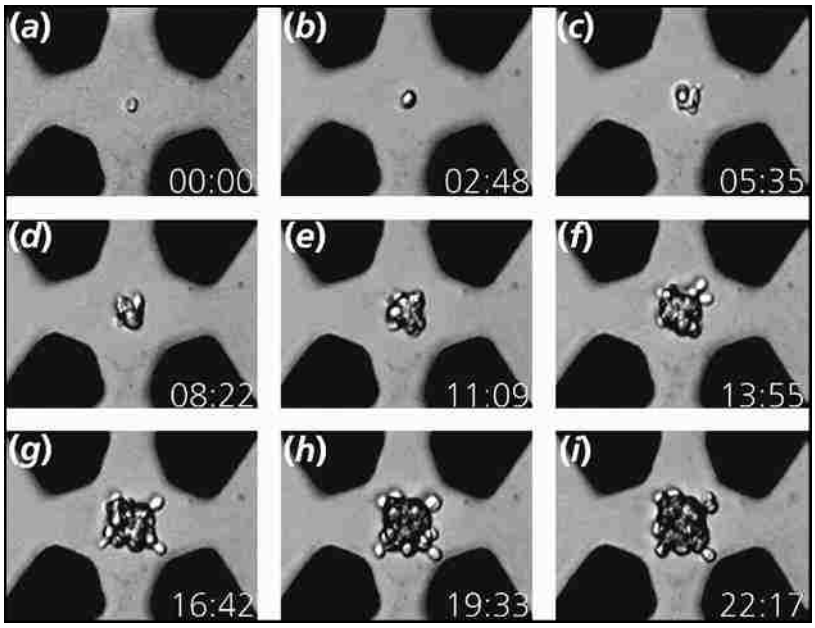

Figure 3.6: Example of yeast proliferation in a DEP cage. Quadruple dark blocks are microelectrodes. The image series show a single trapped yeast cell proliferates into cell agglomerate [115].

3.1.3. Electroosmosis and its applications

Surfaces in contact with an aqueous solution usually have electrostatic charges. The surface charges in turn attract the counter-ions in the liquid to a region close to the surface, forming an electric double layer (DEL) [116-117]. For a fixed solid surface, such as electrodes, the Coulombic force on the predominant counter-ions in the diffuse layer leads to a net migration of the mobile ions in the EDL. The momentum is transported to the adjacent and bulk liquid by viscosity, resulting in an electroosmotic flow (EOF). The

equations describing the velocity field, $\mathbf{u}$, due to electroosmotic flow are those of momentum conservation [117]:

$$\rho_0\left(\partial_t\mathbf{u}+\mathbf{u}\cdot\nabla\mathbf{u}\right)=-\nabla p+\mu\nabla^2\mathbf{u}-\rho_e\nabla\phi \tag{3.7}$$

and continuity:

$$\nabla\cdot\mathbf{u}=0 \tag{3.8}$$

where ρ_0 and μ are the density and viscosity of the fluid, p is the fluid pressure, ϕ is the electric potential, and ρ_e is the charge density in the EDL, given by Poisson's equation

$$\varepsilon\nabla^2\phi=-4\pi\rho_e \tag{3.9}$$

Applying the Debye-Hückel approximation $\phi<<k_BT/e$, the electric potential ϕ is determined by the following Poisson-Boltzmann equation,

$$\nabla^2\phi=-\kappa^2\phi \tag{3.10}$$

where k_B is the Boltzmann constant, T is the absolute temperature, e is the electron charge and κ is a constant determined by the ionic composition of the electrolyte [116]. The Debye length is defined by $\lambda_D=2\pi/\kappa$. In the limit of thin EDL, Eqs. (3.7) and (3.9) could be simplified as

$$\mu\frac{\partial^2 u}{\partial z^2}+\rho_e E\cong 0 \tag{3.11}$$

$$\rho_e\cong-\frac{\varepsilon}{4\pi}\frac{\partial^2\phi}{\partial z^2} \tag{3.12}$$

where E is the external electric field. On eliminating ρ_e between Eqs. (3.9) and (3.10), integrating the resulting differential equation and using the boundary conditions at the

inner and outer edges of the EDL, the following jump condition across the EDL is derived

$$\mathbf{u} - \mathbf{u}_{solid} \equiv \Delta\mathbf{u} = -\frac{\varepsilon \mathbf{E} \varsigma}{4\pi\mu} \tag{3.13}$$

where $\mathbf{u}_{solid}$ is the velocity of the solid at a point on the solid-fluid interface and $\mathbf{u}$ is the velocity of the fluid at the corresponding point [117]. Since electroosmotic flow is generated at the surface-solution interface in a capillary or microfabricated channel, the magnitude of EOF would change due to changes in the chemical composition of the surface, the pH and buffer compositions, and temperature [118].

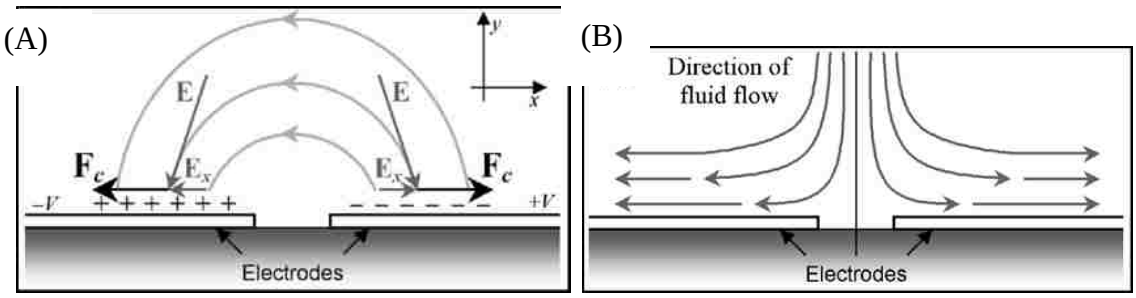

Figure 3.7: Schematic of the mechanism of EOF: (A) Coulombic force on ions due to tangential component E_x on the surface of electrodes; (B) EOF pattern due to ion immigration. [119]

Figure 3.7 shows a schematic of the mechanism of EOF in a typical two planar electrode microdevice. The electrodes are separated by a thin gap in an electrolyte solution. After applying electric field, these two electrodes are subject to different electric potentials. Ions with a sign opposite to electrode charge would accumulate in the EDL on the surface of electrodes. Due to the tangential component of the electric field, a force directed from the center of the gap on the electrode surface would raise, which drives the fluid at the level of the electrodes [119]. It should be noted that this force has a direction

that is independent of the sign of the electrode potential, which indicates EOF in electrolytic solution is steady.

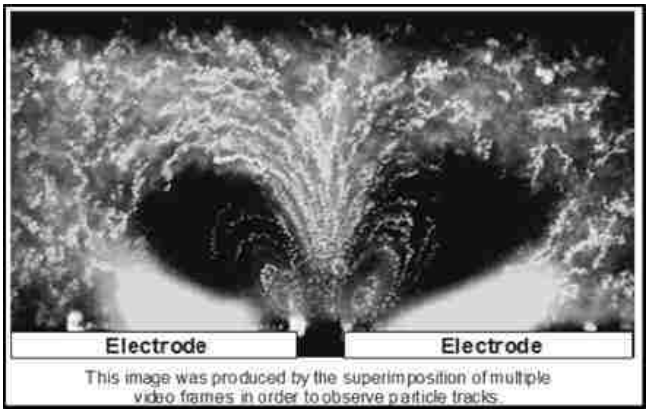

Figure 3.8: Composite image of multiple frames showing particle motion induced by EOF [119].

The experimental observation of the streamlines of a steady electroosmotic fluid flow is presented in Figure 3.8. It clearly shows that the fluid circulates in two symmetrical rolls with the fastest velocities close to the electrode edges. As the distance from the edges increases, the velocity decreases rapidly. Thus, particles far away (at the edge of the image) move more slowly and demonstrate Brownian motion. In addition, as the frequency of AC electric field is decreased, the fluid velocity at the electrode edge remains constant or decreases slightly. However, the rate of decreases of velocity with distance over the electrodes is less, resulting in the center of the streamlines moving further away from the electrode edge over the surface [119].

EOF is also widely used for colloidal self-assembly near electrodes. Nadal *et al.* studied the colloidal aggregation of latex particles on a conducting surface driven by electroosmotic flow [120]. Yeh *et al.* observed the distortions of flow owning to the inhomogeneities in the EDL of ions and couter-ions at the electrode surface, and

demonstrated the potential of applying EOF to assemble microbeads [121]. Lian *et al.* applied EOF on directed depositing and line patterning of particles [122]. When AC signals are applied over the electrodes, non-uniform and synchronous electric fields both normal and tangential to the electrodes are generated to induce microflows, which help the formation of two particles lines on the isolated pair of electrodes, as shown in Figure 3.9.

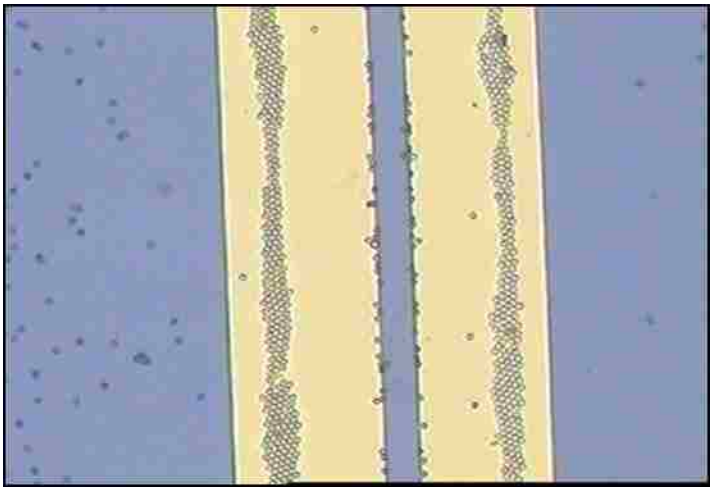

Figure 3.9: Experimental observation of assembly of particle lines due to EOF [122].

Besides the applications in manipulating particles or cells, EOF could also be used to transport bulk fluid into microdevices, in terms of electroosmotic pumps (EOPs). The advantages of EOPs include the creation of pulse-free flows, convenient control of flow magnitude and direction and standard microfabrication technologies. EOPs have so far been used in various areas, such as high performance liquid chromatography (HPLC) separations [123], microelectronic equipment cooling [124], drug delivery [125], and device actuation [126].

In summary, electrokinetics, due to its simple working principles and convenient experimental setups, are becoming one of the most promising techniques for control and manipulation in the microfluidics-based lab-on-a-chip devices. The electrokinetic phenomena, including electrophoresis, dielectrophoresis, and electroosmosis, as described above, have been demonstrated to significantly influence the behavior and movement of cell and biomolecules. In the biosensing community, it has been shown that the response time of DNA microarrays can be enhanced under low pH and low salt concentration, where the surface is positively charged. DNA hybridization rates of 1 nM concentration increase by 80-fold [127]. Therefore, it is very likely that electrokinetic effects would contribute greatly to the three orders' detection time discrepancy at femtomolar concentration between experimental results and theoretical predictions, which are explored in the following sections.

3.2 Mathematical model of biomolecular detection with electrokinetic effects

Factors that would enhance biomolecular detection speed and lead to the large discrepancy of detection time between experiments and theoretical analysis, like the flow rate and statistical variations, have been studied by other researchers [87, 91, 97], but satisfying explanations have not been obtained yet. Lots of reports are published to claim the substantial electrokinetic phenomena on the control and manipulation of biomolecules, but systematical study of electrokinetics for SiNW sensor systems has not been seen until recently. In what follows, a rigorous mathematical model of biomolecular detection with electrokinetic effects is presented, and corresponding numerical

simulations are performed to study the electrokinetic effects on biomolecular detection system.

Based on the existing diffusion theory or Brownian dynamics, the movement of biomolecules is determined by:

$$m\dot{v}_i = \mathbf{f}_i^B \tag{3.14}$$

where m is the mass of each biomolecule, $\dot{v}_i$ is the acceleration for the i_{th} biomolecule and $\mathbf{f}_i^B$ is the force due to Brownian motion that satisfies $\left\langle \mathbf{f}_i^B \right\rangle = 0$ and $\left\langle \mathbf{f}_i^B(t_1)\mathbf{f}_j^B(t_2) \right\rangle = 2k_B T\varsigma\delta_{ij}/\delta t\ \mathbf{I}$. This equation works well in predicating biomolecular detection process in SiNW sensors at high concentration, but the accuracy vanishes at ultralow concentration. Specifically, there exists a three orders' magnitude of detection time difference at femtomolar concentration, which indicates that other factors must be accelerating the biomolecular detection process.

The electrokinetic effects in the SiNW sensing devices are largely due to the applied electric potential on the solution gate. Charged biomolecules move toward the nanowire surface under external electric field, due to the Coulombic force, generated by the interaction between charged biomolecules and the applied electric field, given by

$$\mathbf{F}_{EP,i} = \mathbf{E}_i q \tag{3.15}$$

where $F_{EP,i}$ is the electrophoretic force on the i_{th} biomolecule, $\mathbf{E}_i$ is the strength of electric field at the position of the i_{th} biomolecule and q is the effective charge. In the case that the applied voltage is AC, dielectrophoretic force would arise due to polarization of biomolecules in a non-uniform electric field, given as

$$\mathbf{F}_{DEP,i} = 2\pi\varepsilon_m a_i^3 \cdot \mathbf{K}_{CM,i} \cdot \nabla\left|\mathbf{E}_i\right|^2 \tag{3.16}$$

where $F_{DEP,i}$ is the dielectrophoretic force on the i_{th} biomolecule, ε_m is the permittivity of the medium, a_i is the radius and $\mathbf{K}_{CM,i}$ is the Clausius-Mossotti (CM) factor of the i_{th} biomolecule. Furthermore, at the interface between electrode surface and electrolyte solution, EOF would form in the solution, which can be treated as a slip boundary, given as:

$$\mathbf{u}_{EOF} = -\varepsilon_m \varsigma \mathbf{E}/4\pi\mu \tag{3.17}$$

where ς is the zeta potential, μ is the fluid viscosity. Combining all these factors together, the equation of motion for i_{th} biomolecule can be written as:

$$m\dot{v}_i = -\xi\left(\mathbf{v}_i - \mathbf{u}_f\right) + \mathbf{f}_i^B + q\mathbf{E}_i + 2\pi\varepsilon_m a_i^3 \cdot \mathbf{K}_{CM,i} \cdot \nabla\left|\mathbf{E}_i\right|^2 \tag{3.18}$$

where ξ is the drag coefficient and $\mathbf{u}_f$ is the velocity of the bulk fluid. In most of situations, the applied voltage is DC, which indicates the dielectrophoretic force doesn't need considering, and Eq. (3.18) could be simplified as

$$m\dot{v}_i = -\xi\left(\mathbf{v}_i - \mathbf{u}_f\right) + \mathbf{f}_i^B + q\mathbf{E}_i \tag{3.19}$$

Eqs. (3.18) and (3.19) seem simple, but the exact solutions are difficult to obtain due to the complexity of the system and coupling effects between different forces. Therefore, approximate solutions based on numerical simulations are derived to characterize the electrokinetic effects in SiNW sensors. It should be mentioned that many efforts have already been devoted to study electrokinetic effects numerically. For example, Liu *et al.* developed a computational method "Immersed Finite Element Method" to investigate the electrodeformation of cell, virus detection using dielectrophoretic force and CNT rotation

due to electroosmotic flow [128-131]. Figure 3.10 shows the EOF induced by a DC or low frequency AC field on a pair of parallel rectangular-shaped electrodes with a 5 μm gap. The EOF near the edges of electrodes could induce vortices and rotate suspending nanotubes, which is in good accordance with experimental observations [128].

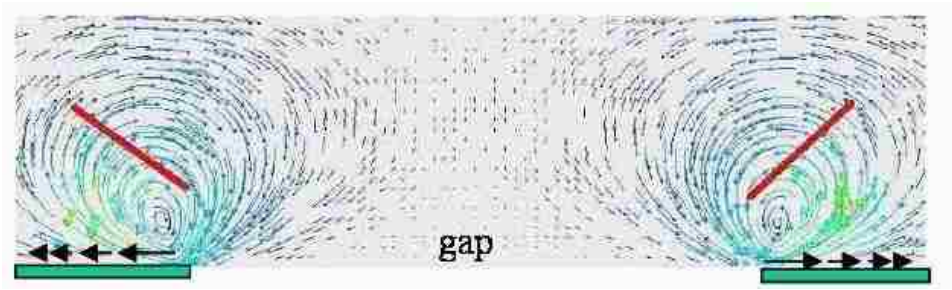

Figure 3.10: Attraction and rotation of nanotubes induced by electroosmotic flow through immersed finite element method [128].

Currently, one of the most common platforms for computational modeling of electrokinetic phenomena has been COMSOL Multiphysics®. Based on its customized electrokinetic module, researchers could directly modify relevant parameters and study various electrokinetic effects in microfluidic devices. For example, Zhang *et al.* presented a numerical investigation of the non-uniform electric fields, created by planar microfabricated electrodes on accelerated transport and capture of virus to a surface inside media of physiological ionic strength [132]. Cheng *et al.* developed a model for electrodeposition of charged nanoparticle on fuel cell coolant flow channel walls, in which electrokinetic force, hydrodynamic force and buoyancy forces were all considered [133]. Davison *et al.* modeled the nanowire trajectories caused by electrokinetic forces using ALE moving mesh in COMSOL Multiphysics® [134]. Here, we would use COMSOL Multiphysics® to model and analyze the electrokinetic effects in SiNW sensing devices.

3.3 Modeling electrokinetic effects in biomolecular detection

In order to characterize the electrokinetic effects on biomolecular detection process and thus establish basic rules to optimize SiNW sensing devices, a multiphysics computational model is developed for systematical study of the SiNW sensor. The geometry of the SiNW sensor is already shown in Figure 2.4. The multiphysics model contains two parts, one is the electric field due to gate voltage, and the other is the velocity field. To solve the electric field, a voltage of -1 V is applied on the solution gate. The surfaces of nanowire are assumed to be ground and other surfaces are assumed to be electric insulation. To solve the velocity field, the bottom surface is assumed to be wall with electroosmotic flow. Other surfaces are assumed to be wall without slip. The density of the fluid is set to be 10^3 kg/m^3. The dynamic viscosity is set to be 10^{-3} Pa·s and the zeta potential is set to be -35 mV. The computational model contains around 100, 000 elements, and it takes half an hour in a workstation with four Intel(R) Xeon(R) CPUs and a memory of 6 GB to finish the simulation.

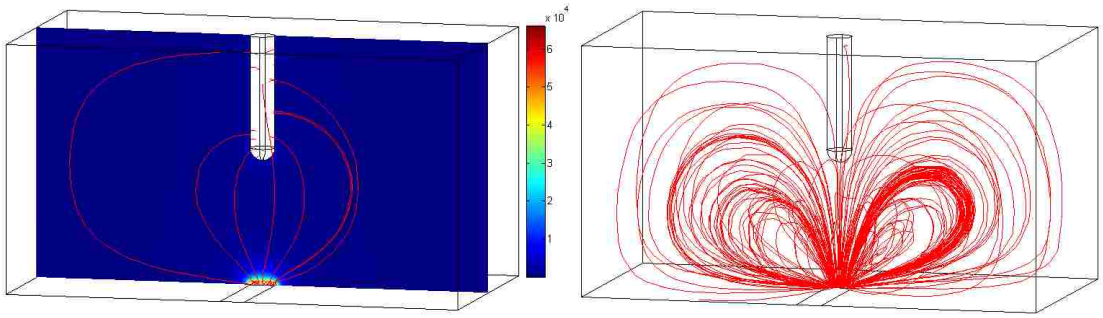

(A) (B)

Figure 3.11: (A) Electric field distribution and (B) electroosmotic flow pattern in SiNW sensors. Streamlines are plotted in red, and the slice shows the magnitude of electric field.

The electric field and velocity field in a typical SiNW sensor are shown in Figure 3.11. The electric field around the nanowire has the highest magnitude, and the strength of the electric field decreases dramatically at positions far away from the nanowire surface. In addition, the streamlines of electric field in Figure 3.11(A) start from the surface of solution gate and end at the surface of nanowire, which indicates the biomolecules might bind on the surface of nanowire if only electrostatic force is considered for their movements. Therefore, when a biomolecule stays far away from the nanowire, the Brownian force dominates the motion of biomolecules, since the electrostatic force is almost negligible under this circumstance. However, when the biomolecule is in the region nearby the sensor surface, the strong electric field that directs toward the sensor surface would help biomolecules bind with receptors on the nanowire surface in a short time. As for the electroosmotic flow shown in Figure 3.11(B), vortexes are generated to circulate biomolecules across the whole fluid domain. Some biomolecules might move close to the nanowire surface owing to electroosmotic flow, while others could be repelled away from the binding region. The overall effect of such vortex generated by electroosmotic flow is the transport of biomolecules in the long range. Compared with electroosmotic flow, the electrostatic attraction is localized near the nanowire surface. If these two effects take place at the same time, it is expected that biomolecules are transported toward the sensing region due to electroosmotic flow, attracted by electrostatic force and then bind with specific receptors on the nanowire surface. Thus, considering the electrokinetic effects, the biomolecular detection time might be greatly reduced.

3.4 Breaking the limits – biomolecular detection with electrokinetic effects

3.4.1. Influence of electrokinetic forces on trajectories of biomolecules

Brownian motion indicates the movement of biomolecules is random and stochastic, which is the leading reason for the long detection time for transporting biomolecules toward the nanowire surface. However, due to electrokinetic forces induced by the existence of solution gate, the random motion of biomolecules would become suppressed to some extent, especially at the region where electrokinetic forces overwhelm the Brownian motion force, and thus the significant reduction of detection time would be expected.

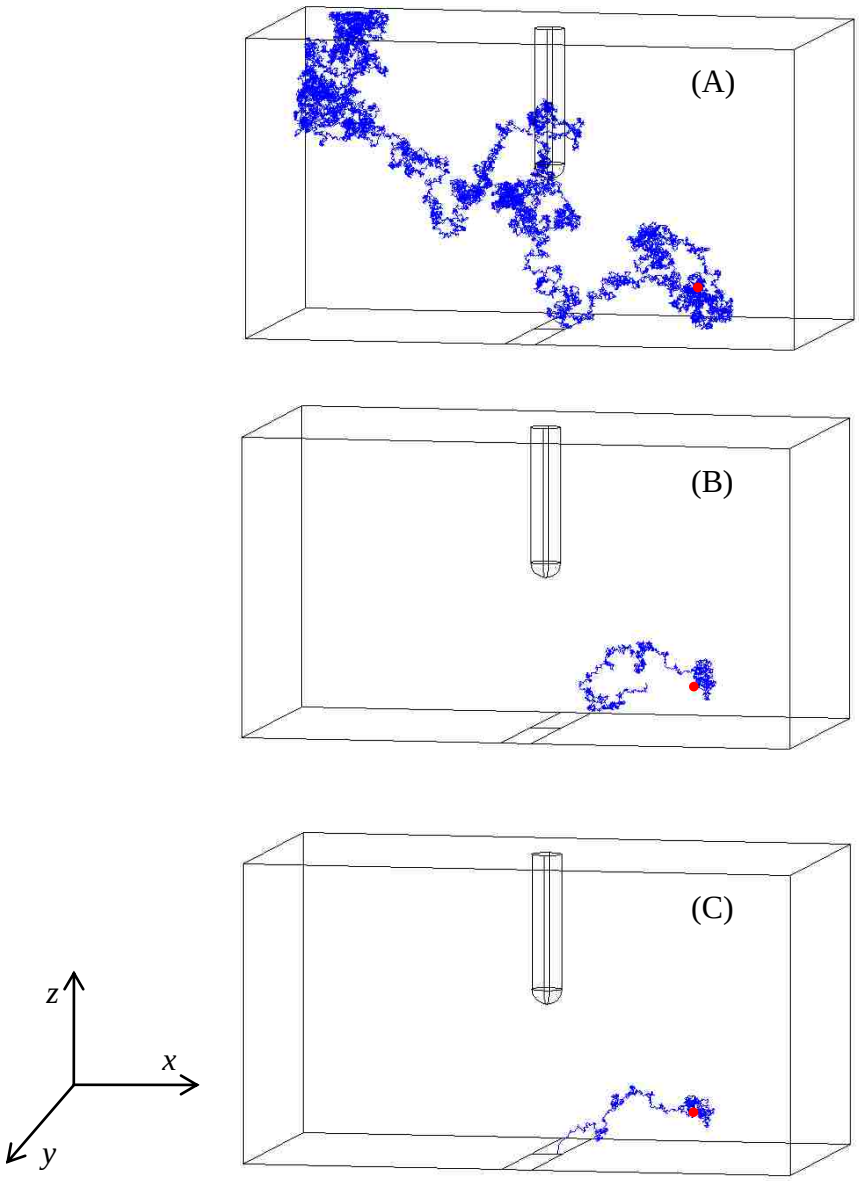

Figure 3.12: Typical trajectories of biomolecules under different effects: (A) Pure Brownian motion (BM); (B) BM and electroosmotic flow (BM&EO); (C) BM, electroosmotic flow and electrophoretic force (BM&EO&EP). The initial positions of biomolecules are represented by red dots. The trajectories are represented by blue lines.

Figure 3.12 shows the typical trajectories of biomolecules under different effects: 1) Pure Brownian motion (BM), 2) BM and electroosmotic flow (BM&EO), and 3) BM,

electroosmotic flow and electrophoretic force (BM&EO&EP). The initial position of the biomolecules in all cases is (100 μm, 0 μm, 30 μm). In the Figure 3.12(A), due to Brownian motion, biomolecules diffuse randomly through the whole domain before they get bound with the nanowire surface, which is a time-consuming process. However, electrokinetic effects would suppress the randomness of the biomolecules' movement and accelerate the detection process. Figure 3.12(B) illustrates a typical trajectory of biomolecules when the influence of electroosmotic flow is considered. Initially, the magnitude of electroosmotic flow is negligible due to the long distance away from the nanowire. The biomolecule is governed by Brownian motion force and the characteristic of the movement is random. As the biomolecule moves close to nanowire, the electroosmotic flow would play an increasingly important role and transport the biomolecule along the vortex flow pattern. If strong electrophoretic force exists nearby the nanowire surface, when the biomolecule circulates close to the sensing region, the biomolecule would be quickly attracted to the nanowire surface, as shown in Figure 3.12(C).

3.4.2. Influence of electrokinetic forces on biomolecular detection time in SiNW sensors

After obtaining the electric field and velocity field from the multiphysics model in COMSOL Multiphysics®, MATLAB® is used to combine these electrokinetic effects and the Brownian motion force together to solve Eq. (3.19) numerically. The number of the biomolecules in the simulation is determined by the analyte concentration. For example, there would be 8950 biomolecules in the model at the 1 pM concentration.

These biomolecules are randomly distributed in the model as the initial configuration at the beginning of simulations. In addition, three binding events are assumed to be enough to trigger an electrical signal.

In the calculation of electrophoretic force on biomolecules, effective charges are used instead of net charges. This is because the ions in the solution induce the screening effect, which makes the interaction force between charged biomolecules smaller than the theoretical calculations based on the net charge. If the ion concentration is in a low level, the screening effect would be weak and there would be no much difference between the net charge and effective charge. Otherwise, the charged biomolecules could be treated as uncharged biomolecules due to high ion concentration in the solution. In the following simulations, two types of biomolecules are considered: one with an effective charge of $10\ e$ and the other of zero effective charge. For charged biomolecules, their movements are affected by the Brownian motion force, the electrophoretic force and electroosmotic flow. For uncharged biomolecules, their movements are determined by the Brownian motion force and electroosmotic flow.

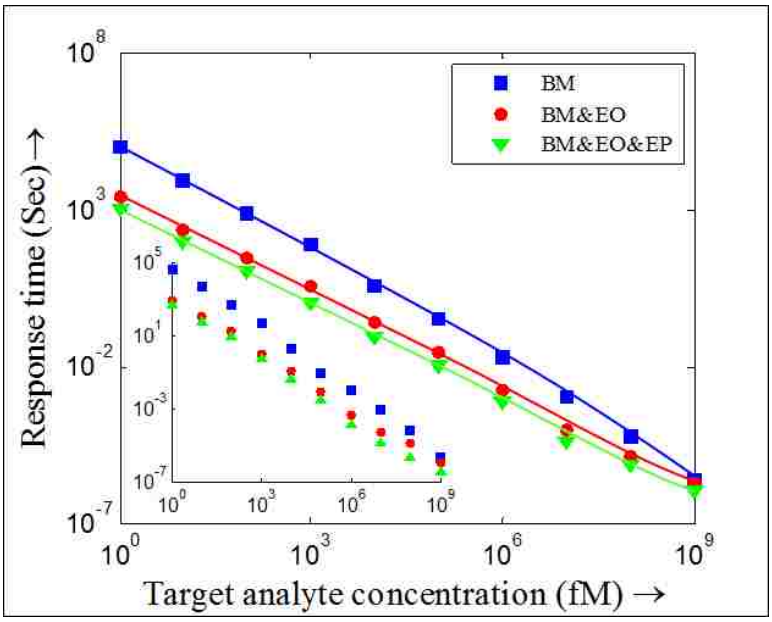

Figure 3.13: Response time of SiNW sensors with electrokinetic effects as a function of analyte concentration. The inset shows the statistical variations of detection time.

Figure 3.13 shows response time of SiNW sensors after considering electrokinetic effects at different concentrations. If only Brownian motion of biomolecules is considered, the response time decreases with the increase of concentrations with a slope of -1 in logarithm at sub-fM concentration. The slope changes to be around -1.5 at high concentration. This phenomenon may be due to the decrease of average distance between biomolecules and nanowire surfaces. At high concentration, the distance between nanowire surfaces and biomolecules is short, especially for the first few biomolecules bound with the nanowire surface. The closer the biomolecules are to the nanowire surface, the more likely that SiNW sensors would perform like planar sensors, and the slope would keep decreasing until it approaches the limit of -2, which is the slope in logarithm between the detection time and analyte concentration in 1D planar sensor. Significant reduction in response time is observed after introducing electrokinetic effects. At concentration 1 fM, the response time difference is around 41 times for uncharged

biomolecules, and around 93 times for charged biomolecules. Such difference in detection time induced by electrokinetic effects vanishes at high concentration of around 1 μM. This is because the distance for biomolecules to travel and bind with the sensor surface decreases as the concentration increases. Beyond a certain analyte concentration, the Brownian motion becomes the dominant factor to deliver biomolecules toward the nanowire surface. Such observation indicates that the diffusion-reaction theory is only valid at medium or high concentration while electrokinetic effects should be taken into account at ultralow concentration (less than 1 μM).

Electrokinetic effects, especially for charged biomolecules, could accelerate detection process up to 93 times in a typical SiNW sensor with a single nanowire of diameter 100 nm and length 20 μm. This is encouraging because there are just 10 times of detection time difference left between experimental results and theoretical calculations. We believe other factors, such as the size of nanowires, biomolecular charge, would account for remaining detection time difference. Therefore, some important factors that might influence biomolecular detection process, including nanowire design, solution gate design and biomolecular charge, are characterized in the following section for fully resolving the puzzle of detection time discrepancy at ultralow concentration.

Chapter 4

Design considerations of SiNW sensors under electrokinetic effects

This chapter describes the design considerations of the SiNW sensor in detecting biomolecules under electrokinetic effects. The chapter 3 has already demonstrated the significant acceleration of biomolecular detection process due to electrokinetic forces. The three orders' gap of detection time between experimental results and theoretical calculations is decreased by over ninety times for biomolecules with effective charge 10 e in a typical SiNW sensor device with a nanowire of diameter 100 nm and length 20 μm. The remaining ten times difference of detection time is expected due to the design of SiNW sensors. In what follows, an introduction about previous studies on SiNW sensor design is presented. Then the influences of several factors, including nanowire design, solution gate design and biomolecular charge, on the biomolecular detection process using SiNW sensors, are investigated and discussed in detail. The chapter is concluded with an explanation of the three orders of magnitude of detection time discrepancy and a discussion about the optimal design for improving the performance of SiNW sensors.

4.1 Design considerations of SiNW sensors

SiNW sensors can provide fast, low-cost, ultrasensitive, and high-throughput analysis of biological systems, which has already been demonstrated by various groups [65, 85, 89]. Despite these advancements, the design principles of SiNW sensors are still

not clearly elaborated, and thus the further optimization of SiNW sensors for better performance is hindered. Generally, nanowires with lower doping density and smaller diameter could provide better sensitivity, due to their high surface-to-volume ratio. Nair *et al.* studied the prospects and challenges of biomolecular detection using SiNW biosensors as a function of device parameters, as shown in Figure 4.1 [135]. It clearly shows that sensitivity increases with smaller diameter and reduced doping density. The reduced nanowire length could also increase the relative sensitivity significantly, particularly for higher doping densities, as shown in Figure 4.1(B). Therefore, it seems that any desired sensitivity could be achieved by choosing smaller length, diameter, and reduced doping density. However, this is not correct. Apart from the technological difficulties associated with the continued scaling of dimensions, doping also can't be reduced to low values without introducing significant variation in sensor performance, which is referred to as discrete dopant fluctuations in nanoscale transistor design [136]. A lower limit to doping density exists, below which discrete dopant fluctuation causes unpredictable variation of baseline sensitivity, making it impossible to integrate them in an array format.

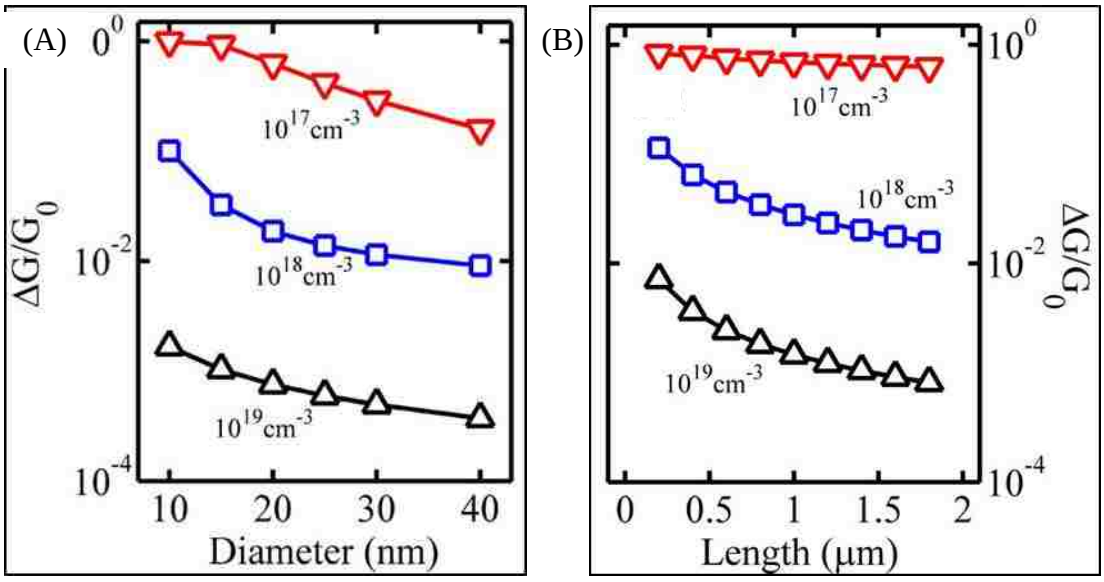

Figure 4.1: Sensitivity of SiNW sensors as a function of diameter (A) and length (B) with different doping density [135].

In addition, small diameter and length of nanowire would retard the speed for accumulation of biomolecules on a nanowire surface. Sheehan *et al.* examined the performance of a cylindrical sensor oriented perpendicular to a channel, as shown in Figure 4.2. The tradeoff between the required time to accumulate certain number of biomolecules and the radius of nanowires is studied at 1 fM concentration. As the size of the nanowire decreases to 10 nm, the time to accumulate several biomolecules could reach several days, which is unacceptable due to the stability of the measurement. Other factors, such as nonspecific binding, sample degradation, and stochastic nature of measuring only a few molecules would make accurate measurement difficult. The situation worsens for SiNW sensors with short nanowires [87].

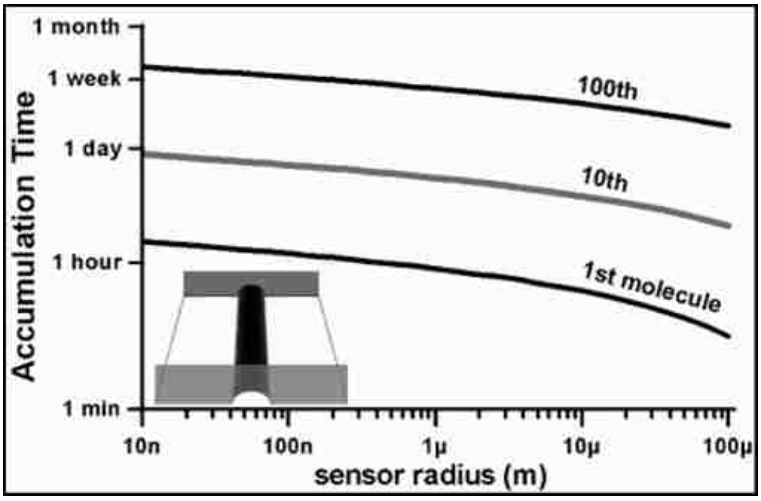

Figure 4.2: Time required for a 10 µm long hemicylindrical sensor to accumulate 1, 10, and 100 biomolecules as a function of nanowire radius [87].

Instead of taking several days to accumulate several biomolecules on nanowire surfaces at fM concentration, experimental results show that it just needs several minutes to finish the biomolecular detection process, which indicates the above design principles are not accurate and new rules to guide the SiNW sensor design should be developed to help further advancement of SiNW sensors of higher performance. Electrokinetic effects, due to applied DC voltage on solution gate, could lead to enhance the biomolecular detection speed by over one hundred times in a typical single-nanowire biosensor. Therefore, it is possible that appropriate SiNW design, combined with the speed acceleration due to electrokinetic forces, would lead the three-order magnitude of detection time difference.

4.2 Influence of nanowire design on biomolecular detection process

Charged biomolecules bind with nanowire surface and change the conductance/resistance of nanowires, which triggers a detectable signal. It is thus important to characterize how the nanowire design would affect the biomolecular binding

process. The size of nanowire, which is closely relevant with the sensitivity of SiNW devices, and the nanowire array, which is designed for multiplexed detection of biomolecules, are investigated under electrokinetic effects using our multiphysics computational model.

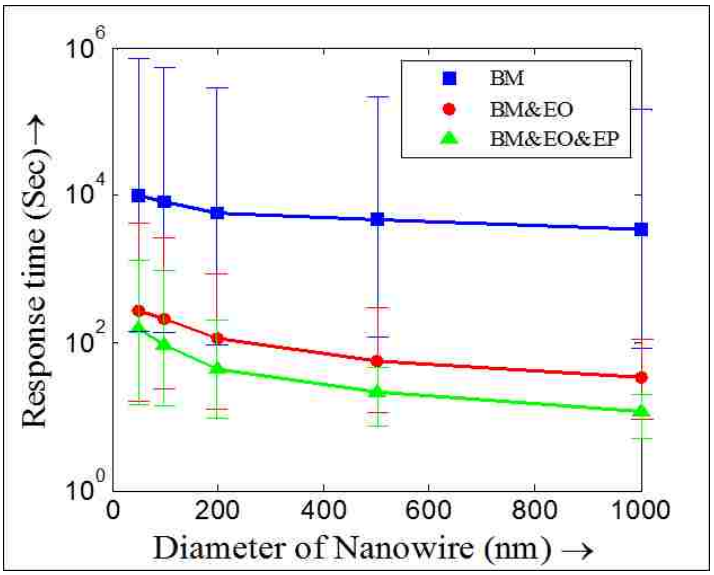

Figure 4.3: Response time under electrokinetic effects for SiNW sensors with nanowires of different diameters at concentration 10 fM. Statistical variations are plotted as error bars.

Nanowire size could profoundly affect the total analyte flux on nanowire surfaces. Sheehan *et al.* studied the detection efficiency of nanowire biosensor in unmixed fluids with size from the micrometer to nanometer scale, and claimed that fM detection limits for biomolecular assays are very likely an analyte transport limited process, not a signal transduction limited process [87]. However, Sheehan's conclusions are based on the pure diffusion theory without considering electrokinetic effects, which, we believe, is the leading reason for the discrepancy of detection time at femtomolar concentration. Here, we reinvestigate the influence of nanowire size on the biomolecular detection process. The diameter of nanowires is varied from 50 nm to 1 μm, and the accumulation time for

collecting three biomolecules are recorded, as shown in Figure 4.3. The detection time decreases with the increase of nanowire diameter. This is because the larger the diameter of the nanowire is, the larger surface is available for binding reactions, thus causes a reduction in the detection time. Under pure Brownian motion, the detection time decreases from 1.014×10^4 seconds to 3.557×10^3 seconds, when the diameter of nanowires increases from 50 nm to 1 μm. In other words, twenty times change in diameter of nanowires just induces less than three times change in detection time. This weak relationship is in accordance with the predictions from diffusion-reaction theory [87]. Considering electrokinetic effects, the detection time is subject to a significant reduction, which is around 64 times for charged biomolecules and 37 times for uncharged biomolecules when the nanowire has a diameter of 50 nm. This gap increases to 309 times for charged biomolecules and 105 times for uncharged biomolecules as the diameter increases to 1 μm, which indicates SiNW sensor should have a nanowire of large diameter in order to accumulate more biomolecules in a certain time at sub-fM concentration. Of course, large diameter means small surface-to-volume ratio and low sensitivity of SiNW sensors. Therefore, for the SiNW sensors with similar sensitivity, the nanowire with larger diameter could give a detection signal in a shorter time and thus is a better option for SiNW sensor design.

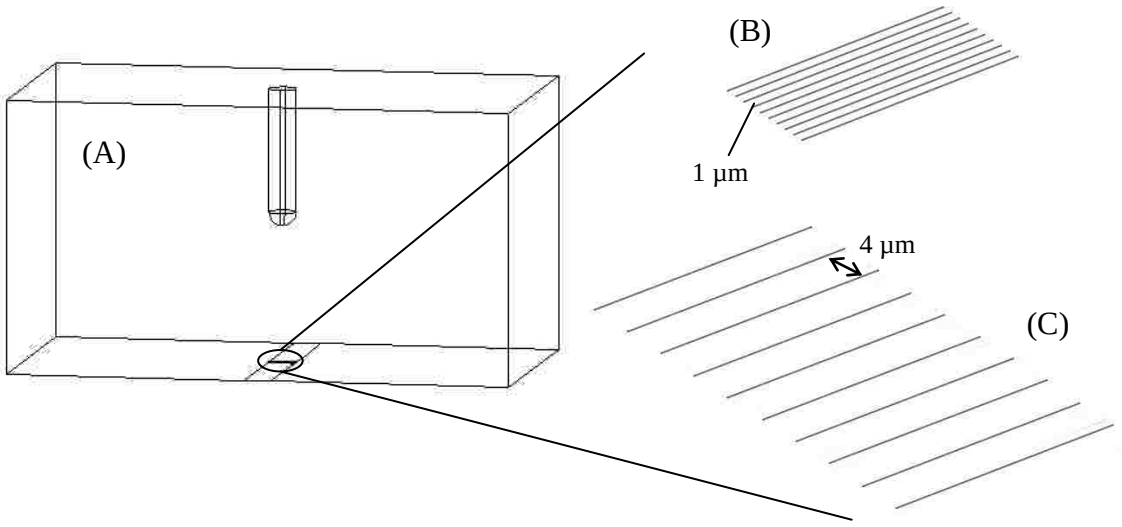

Figure 4.4: (A) Configuration of SiNW sensor with multiple nanowires; (B) 10-nanowire array with 1 µm separation distance; (C) 10-nanowire array with 4 µm separation distance.

Another important design concern about SiNW sensor is the number of nanowires. Nanowire array could be used for detecting of multiple disease marker proteins simultaneously in a single, versatile detection platform [85]. In addition, the use of multiple nanowires instead of a single nanowire as sensing elements enables high device uniformity and stability in buffer solutions and selective detection of bovine serum albumin at concentration as low as 0.1 fM [137]. Thus it is of vital importance to characterize the biomolecular detection process in the nanowire array.

Figure 4.4(A) shows the configuration of the SiNW sensing model with multiple nanowires. These nanowires are patterned in parallel at the bottom surface. The influence of the nanowire number on the biomolecular detection process is studied, as well as the effect of separation distance among nanowires. Figure 4.4(B) and (C) show the configurations of the 10-nanowire array with separation distance 1 µm and 4 µm, respectively.

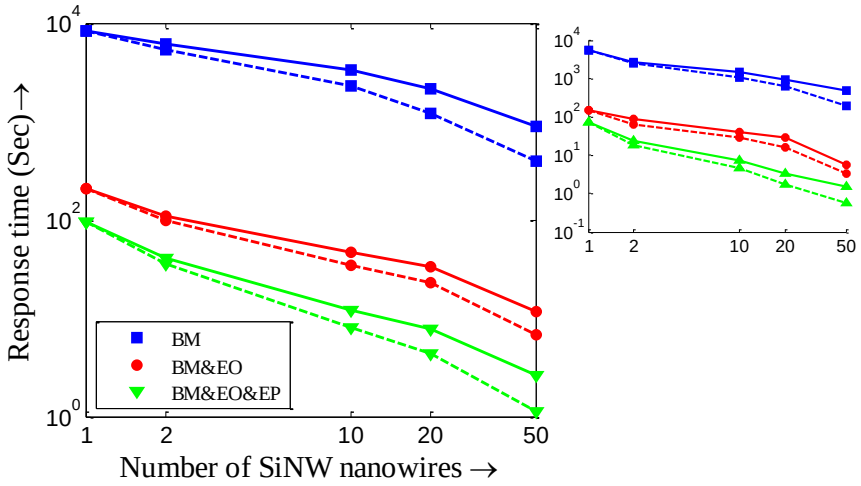

Figure 4.5: Response time under electrokinetic effects for nanowire array with 1, 2, 10, 20, and 50 nanowires at concentration 10 fM. Solid lines represent response time of nanowire array with separation distance 1 μm, and dashed lines represent response time of nanowire array with separation distance 4 μm. The inset shows the statistical variations of detection time.

The increase of nanowire number would add more available sensing surfaces for target biomolecules reacting with receptors on surfaces. Thus the array with large number of nanowires requires less time to accumulate enough binding events to trigger a signal than that with a few nanowires, as shown in Figure 4.5. In the arrays with 1 μm separation distance, the detection time difference between BM and BM&EO increases from 40 times for the single nanowire sensor to 78 times for the 50-nanowire array, whereas, the gap between BM and BM&EO&EP increases from 87 times to 338 times. The same phenomenon happens to the arrays with 4 μm separation distance, there exists around 60 times detection time difference between BM and BM&EO for the 50-nanowire array case, and the response time difference between BM and BM&EO&EP increases to 355 times after the number of nanowires change from 1 to 50. This indicates the acceleration of biomolecular detection process becomes more evident due to the

electrokinetic effects in nanowire arrays. In addition, after altering the separation distance to 4 μm, the detection time decreases, and is almost half of that using 50-nanowire array with 1 μm separation distance. This may be due to the less electrokinetic interference due to other nanowires in the pattern with 4 μm separation distance than that with 1 μm separation distance when one nanowire is going to capture biomolecules nearby. In addition, large separation could spread out nanowire pattern and provide more chance for biomolecules binding with nanowire surfaces. Of course, there is a tradeoff between the number of nanowires and the available sensitivity in SiNW sensing devices. Nanowire array needs capture more target biomolecules to trigger a signal than that in single nanowire devices. However, if increasing the number of nanowires does not severely decrease the sensitivity of SiNW sensor array devices, better performance in detection biomolecules would be achieved by adding more number of nanowires and increasing the separation distance between nanowires.

4.3 Influence of solution gate design on biomolecular detection process

Electrokinetic effects in SiNW sensors are mainly induced by the applied voltage on the solution gate. Two major design concerns, magnitude of applied voltage and the position of solution gate, which may change the electric field and thus the electrokinetic forces, are studied.

Figure 4.6 shows the influence of applied voltage on the solution gate on the biomolecular detection time. The magnitude of electrokinetic forces, including electrophoretic force and electroosmotic flow, is proportional to the applied voltage on

solution gate. When the voltage applied on the solution gate is small, for example, less than 0.01 V, electrokinetic forces are negligible compared with the Brownian force. In this case, the movement of biomolecules is mainly determined by Brownian motion force and the detection time would approach the limits predicted from diffusion-reaction theory. Thus, two lines with small slopes are observed at the low voltage region. As the applied voltage increases, the electrokinetic forces would accelerate the biomolecular detection process and a significant reduction in detection time is observed. The detection time at 10^{-2} V is around 2500 seconds, whereas it decreases to 1 second for charged biomolecules and 3 seconds for uncharged biomolecules at 100 V, which is over one thousand times of detection time difference. Therefore, it seems that a high voltage should be applied on the solution gate to achieve ultrafast detection of target biomolecules. However, the magnitude of applied voltage has some limitations. The main purpose of adding the solution gate in SiNW device is to modulate the conductance of silicon nanowire in an appropriate range, which is sensitive to the electric potential variations on the nanowire surface due to specific biological interactions. Although the applied voltages on solution gate vary with the shape and size of nanowires in sensing devices, a voltage between 0.5 V ~ 10 V is often adopted in experiments [138]. When the voltage increases from 0.5 V to 10 V, the detection time would reduce by ~ 20 times, both for charged biomolecules and uncharged ones. An ultralow or ultrahigh voltage on the solution gate would lead no sensitivity to target biomolecules in SiNW sensing devices. In addition, high voltage would also cause damage to the sensing devices and shorten their life expectancy. Therefore, the role of applied voltage on enhancing

biomolecular detection process is limited, but a higher voltage is preferred for SiNW sensors to perform ultrafast detection if applicable.

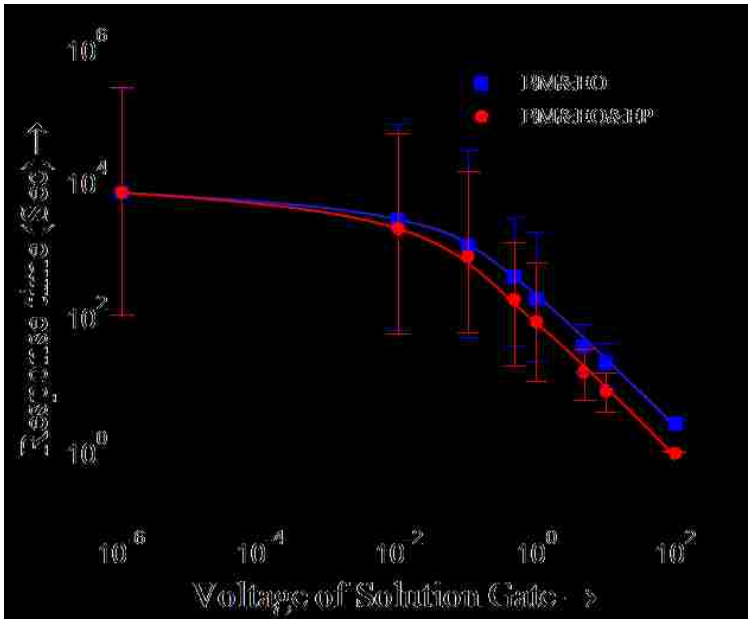

Figure 4.6: Response time under electrokinetic effects for SiNW sensors with solution gate of different voltages, at concentration 10 fM. Statistical variations are plotted as error bars.

The position of solution gate would change the electric field distribution, and thus affect the acceleration of biomolecular detection process due to electrokinetic effects. Here, the effects of the separation distance between the tip of solution gate and the nanowire surface on detection time are studied, as shown in Figure 4.7. Due to the limitation of the model dimension, four different separation distances, 50 μm, 100 μm, 150 μm and 175 μm, are chosen in numerical simulations. The position of the solution gate doesn't affect the biomolecular detection process under pure Brownian motion, thus only the response time under BM&EO, and BM&EO&EP are plotted. The simulation results show two almost flat lines, which means the response time doesn't change with separation distance between the solution gate and the nanowire surface. The electric field

and the electroosmotic velocity at different positions are examined, and no much difference is found for different solution gate designs. Thus electrokinetic forces don't have much change under different solution position, and the slightly variation of detection time due to the change of solution gate positions would be suppressed by the statistical variations of response time. Therefore, we conclude that the influence of the solution gate position in the devices on the detection time could be ignored.

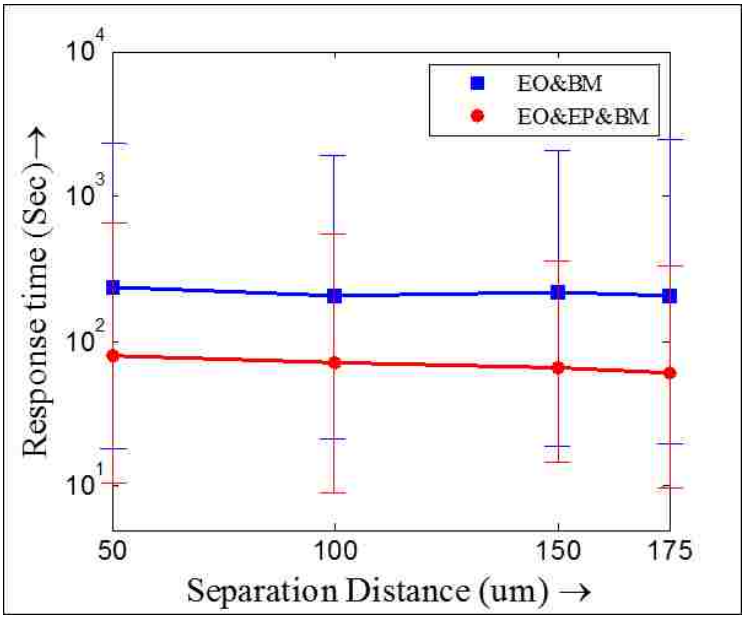

Figure 4.7: Response time under electrokinetic effects for SiNW sensors with different separation distances between solution gate and nanowires, at concentration 10 fM. Statistical variations are plotted as error bars.

4.4 Influence of biomolecular charge on biomolecular detection process

Many biomolecules carry an electrostatic charge under normal physiological conditions. DNA is negatively charged. For a protein, the effective charge depends on the pH of the solution and can be estimated using Henderson-Hasselbalch equation and the dissociation constants of the amino acids which constituted the protein [139]. The pH at

which the effective charge of protein becomes zero is called its isoelectric point [140]. Above the isoelectric point, the protein has a negative charge, and the charge increases as the pH increases, which would greatly affect the response time in SiNW sensing devices.

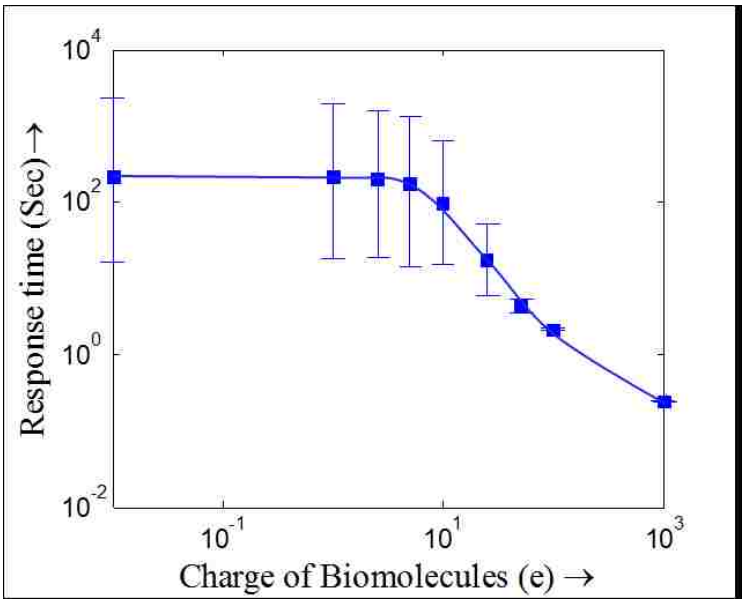

Figure 4.8: Response time for biomolecules with effective charges from 0.01 to 1000 *e*, at concentration 10 fM. Statistical variations are plotted as well.

Figure 4.8 shows the effect of effective charges of biomolecules on the detection time. The applied voltage on the solution gate is kept to be -1 V. Thus, the electroosmotic flow and the detection time under BM&EO would not change during the detection process. However, based on the Coulomb's law, the electrophoretic force would increase proportionally with effective charges of biomolecules. When biomolecules are weekly charged (less than $5e$), electrophoretic force has negligible influence on biomolecular detection process. The response time is determined by Brownian motion force and electroosmotic flow, and a flat line is observed. For biomolecules with an effective charge greater than $5e$, a sharp decrease of detection time happens because electrophoretic force is larger enough to capture biomolecules nearby to the nanowire

surface. Specifically, the detection time for biomolecules with charge $5e$ is around 173 seconds, while it only takes less than 2 seconds for biomolecules with charge $100e$. The detection time difference reaches eighty five times after increasing charge for only twenty times. As the charge of biomolecules continue increasing, the movement of biomolecules would be totally controlled by electrophoretic force and the detection time decreases as a function of the biomolecular charge with a slope around -1 in logarithm. Therefore, to enhance the biomolecular detection process, the influence of fluid environment on biomolecular charge should be carefully considered. For biomolecules in p-SiNW sensing devices, large negative surface charge is desired, whereas in n-SiNW sensors, adding more positive surface charge would help decrease the detection time. The main method to control biomolecular charge is to vary pH value of the solution. However, some side-effects should be considered before modifying pH of the solution. PH value that is too high or too low would cause corrosion of the sensing devices and, most importantly, deactivate target biomolecules, such as protein, in the solution.

So far, SiNW sensing devices with different designs are investigated under electrokinetic effects using the developed multiphysics computational model and it is found that factors, like the nanowire size, nanowire number, applied voltage, and biomolecular charge, could cause substantial reduction of detection time in biomolecular detection process, while the solution gate position has minor influences. The gap of detection time difference between BM and BM&EO&EP could reach 309 times, 338 times in the design with nanowire of diameter 1 μm and 50-nanowire sensing array, respectively. In addition, the detection time would decrease over one thousand times after changing the applied voltage from 10^{-2} V to 100 V, and around 85 times after increase the

effective charge of biomolecules from $5e$ to $100e$. Therefore, the combined effects of electrokinetic forces, large size of nanowire, multiple nanowires, high applied voltage, and large surface charge of biomolecules could easily decrease detection time by three orders of magnitude compared with that given by diffusion-reaction theory. The optimization of SiNW sensor could be achieved by introducing nanowire of large diameter, more number of nanowires with large separation distance, high gate voltage and appropriate solution environment to maximize the biomolecular surface charge.

Chapter 5

Conclusions

5.1 Conclusions

In this thesis, a multiphysics computational model has been developed to study the biomolecular detection process with electrokinetic effects using SiNW sensors. SiNW sensors are becoming the most powerful tool to quantify and analyze biological samples. Compared with optical biosensors, SiNW sensors could be miniaturized into the nano-scale size, which makes them suitable for multiplexed detection of biomolecules in a single clinic sample. Compared with planar sensors (ISFET), SiNW sensors provide ultrahigh sensitivity, and have the potential to register an electrical signal in the presence of one single target biomolecule, due to the high surface-to-volume ratio. Compared with CNTs, SiNW sensors have mature fabrication techniques and simple sensing mechanism. Together with other inherent advantages, such as label-free and real-time detection and high selectivity, SiNW sensors has been demonstrated to be an excellent platform for detecting various biomolecules, and thus it is crucial to characterize SiNW sensing systems for developing biosensors of higher performance and reliability.

Traditional computational models for predicting the performance of SiNW sensors are based on the diffusion-reaction theory. This theory studies the ensemble average of the stochastic behavior of biomolecules. It works quite well in predicting the behaviors of biomolecules at high concentration, but there exists three orders of magnitude of

detection time difference between theoretical predictions and experimental results. Other theories, such as convection-diffusion-reaction theory and statistical variance theory, could not explain this puzzle either. This discrepancy is also demonstrated by our computational model based on Brownian dynamics.

Electrokinetic effects, introduced by the applied voltage on solution gate, are explored for their contribution to accelerate the biomolecular detection process using the developed multiphysics computational model. For charged biomolecules, the influences of electrophoretic force, electroosmotic flow and Brownian motion force on biomolecules' movement are considered, while the behavior of uncharged biomolecules is affected by electroosmotic flow and Brownian motion force. In a typical single nanowire biosensor, it is found that the biomolecular detection process is enhanced by over ninety times for charged biomolecules, and over forty times for uncharged biomolecules.

Several design considerations of SiNW sensors, including the nanowire design, solution gate design and biomolecular charge, are investigated based on our computational approach. Over three hundred and nine times of speed acceleration in detecting charged biomolecules could be observed in the SiNW sensor design with a single nanowire of diameter 1 μm. Additionally, nanowire array could introduce more significant reduction of detection time, which is a three hundred and forty times enhancement for charged biomolecules using 50-nanowire array. The comparison between detection time of nanowire arrays with difference separation distances indicates large separation distance is beneficial for ultrafast detection. In addition, the applied voltage on the solution gate and biomolecular charge can also accelerate the detection

speed, but there exist a lot of limitations, such as the conductivity of SiNW and pH value in the solution. The position of the gate is found to have no effect on the biomolecular detection process.

Electrokinetic effects, when combined with SiNW sensor design: large diameter of nanowire, multiple-nanowire array, high applied voltage on solution gate and high surface charge of biomolecules, can well explain the three orders of magnitude difference in biomolecular detection process between experiments and diffusion-reaction theory. The optimal design of SiNW sensor would be achieved by an appropriate combination of these factors, which has nanowires of large diameter and numbers while the sensitivity is slightly degraded. Moreover, high applied voltage on solution gate should be chose if the detection of biological interaction potential using nanowires is not affected. It would also be helpful if the surrounding environment could induce large charges on biomolecules' surface without introducing any serious side-effects.

5.2 Future work

Besides electrophoretic force and electroosmotic flow, other kinds of electrokinetic effects would also possibly accelerate the biomolecular detection process. Specifically, when an AC voltage is applied to the solution gate, DEP force would arise from induced dipole moments on a biomolecule immersed in a non-uniform electric field and provide a short-range attractive force that attracts nearby biomolecules quickly toward the nanowire surface. Since the dielectrophoretic force doesn't require biomolecules to be electrically charged, a further reduction of detection time would be expected for both charged

biomolecules and uncharged ones, which will be demonstrated by our developed multiphysics computational model in the future.

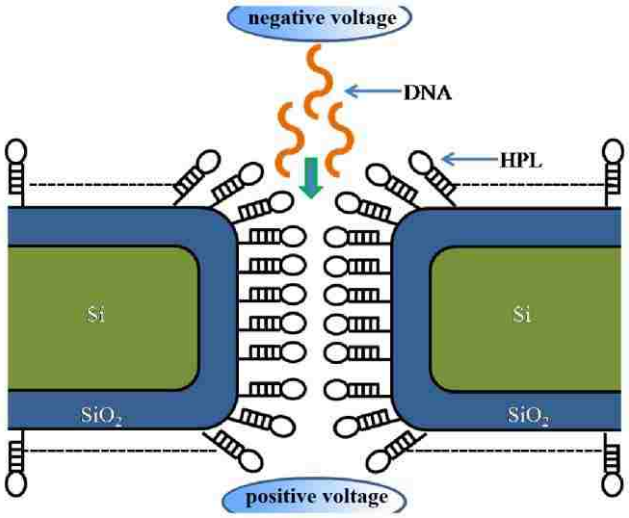

Figure 5.1: Transport of DNA through a nanopore-based sensing system under electric field [141].

Another area that needs to be studied is the interactions between biomolecules and receptors on the sensor surface. The detection signal is triggered by the electric potential variations due to the biological interactions on the sensor surface. Previous studies ignored these interactions and assumed that biomolecules bind with the nanowire surface once they were in contact with each other, which is not the case in experiments. In addition, the influence of electrokinetic forces on the biological interactions at molecular level in SiNW sensing system is rarely studied. In order to characterize these biological interactions under applied electric field and quantify their effects on the whole biomolecular detection process, molecular dynamics simulations need to be performed. The interactions between single strand DNA and hairpin-loop DNA under electric forces in a nanopore-based sensing system had been studied in our group, as shown in Figure

5.1 [141]. The similar computational tool will be applied to study the interactions between target biomolecules and receptors with electrokinetic effects in SiNW biosensors.

Finally, experimental studies will be performed to verify the results from above numerical simulations and provide a framework for understanding the fundamental biosensing mechanism at ultralow concentration and optimizing biosensors to achieve higher sensitivity and ultrafast biomolecular detection. An integrated sensor chip of nanowires of varied widths and number, solution gate of different positions and applied voltages, and biomolecules of different surface charges will be built and be applied to investigate the correlations among detection time, nanowire size, nanowire array, gate voltage and so on. These results will be compared with simulation results for creating a novel biosensing platform of next generation.

Bibliography

1. Chen, K.-I., B.-R. Li, and Y.-T. Chen, *Silicon nanowire field-effect transistor-based biosensors for biomedical diagnosis and cellular recording investigation.* Nano Today, 2011. **6**(2): p. 131-154.

2. Patolsky, F., G. Zheng, and C.M. Lieber, *Nanowire sensors for medicine and the life sciences.* Nanomedicine (London, England), 2006. **1**(1): p. 51-65.

3. Thévenot, D.R., K. Toth, R.A. Durst, and G.S. Wilson, *Electrochemical biosensors: recommended definitions and classification.* Biosensors and Bioelectronics, 2001. **16**(1-2): p. 121-131.

4. Grieshaber, D., R. MacKenzie, J. Vörös, and E. Reimhult, *Electrochemical Biosensors - Sensor Principles and Architectures.* Sensors, 2008. **8**(3): p. 1400-1458.

5. Ghiran, C.I., *Introduction to Fluorescence Microscopy.* Springer, New York, NY, 2011.

6. Wolf, D.E., *Fundamentals of Fluorescence and Fluorescence Microscopy*, in *Methods in Cell Biology*, S. Greenfield and E.W. David, Editors. 2007, Academic Press. p. 63-91.

7. Chen, D.Y., H.P. Swerdlow, H.R. Harke, J.Z. Zhang, and N.J. Dovichi, *Low-cost, high-sensitivity laser-induced fluorescence detection for DNA sequencing by capillary gel electrophoresis.* Journal of Chromatography A, 1991. **559**(1-2): p. 237-246.

8. Abdel-Baky, S. and R.W. Giese, *Gas chromatography/electron capture negative-ion mass spectrometry at the zeptomole level.* Analytical Chemistry, 1991. **63**(24): p. 2986-2989.

9. Murakami, S., K. Ito, T. Goto, S. Kamada, and M. Maeda, *Bioluminescent enzyme immunoassay using thermostable mutant luciferase and acetate kinase as a labelled enzyme.* Analytica Chimica Acta, 1998. **361**(1-2): p. 19-26.

10. Gould, S.J. and S. Subramani, *Firefly luciferase as a tool in molecular and cell biology.* Analytical Biochemistry, 1988. **175**(1): p. 5-13.

11. Sood, A., B.F. Spielvogel, and inventors, *Detection of biopolymers and biooligomers with boron hydride labels.* US patent 5,595,878, 1997.

12. Bruchez, M., M. Moronne, P. Gin, S. Weiss, and A.P. Alivisatos, *Semiconductor Nanocrystals as Fluorescent Biological Labels.* Science, 1998. **281**(5385): p. 2013-2016.

13. Arwin, H., M. Poksinski, and K. Johansen, *Total Internal Reflection Ellipsometry: Principles and Applications.* Appl. Opt., 2004. **43**(15): p. 3028-3036.

14. Luppa, P.B., L.J. Sokoll, and D.W. Chan, *Immunosensors--principles and applications to clinical chemistry.* Clinica Chimica Acta, 2001. **314**(1-2): p. 1-26.

15. Elwing, H., *Protein absorption and ellipsometry in biomaterial research.* Biomaterials, 1998. **19**(4-5): p. 397-406.

16. Goodall, D.G., G.W. Stevens, D. Beaglehole, and M.L. Gee, *Imaging Ellipsometry/Reflectometry for Profiling the Shape of a Deformable Droplet as It Approaches an Interface.* Langmuir, 1999. **15**(13): p. 4579-4583.

17. Liedberg, B., C. Nylander, and I. Lunström, *Surface plasmon resonance for gas detection and biosensing.* Sensors and Actuators, 1983. **4**: p. 299-304.

18. McDonnell, J.M., *Surface plasmon resonance: towards an understanding of the mechanisms of biological molecular recognition.* Current Opinion in Chemical Biology, 2001. **5**(5): p. 572-577.

19. Vörös, J., J.J. Ramsden, G. Csúcs, Szendro, I., S.M. De Paul, M. Textor, and N.D. Spencer, *Optical grating coupler biosensors.* Biomaterials, 2002. **23**(17): p. 3699-3710.

20. O'Sullivan, C.K. and G.G. Guilbault, *Commercial quartz crystal microbalances - theory and applications.* Biosensors and Bioelectronics, 1999. **14**(8-9): p. 663-670.

21. Marx, K., *Quartz crystal microbalance: A useful tool for studying thin polymer films and complexes biomolecular systems at the solution-surface interface.* Bio Macromolecules, 2002. **4**(5): p. 1099-1120.

22. D'Orazio, P., *Biosensors in clinical chemistry.* Clinica Chimica Acta, 2003. **334**(1-2): p. 41-69.

23. Clark, L.C., *Monitor and control of blood and tissue oxygen tensions.* Transactions American Society for Artificial Internal Organs, 1956. **2**(41-&).

24. Santandreu, M., S. Alegret, and E. Fàbregas, *Determination of [beta]-HCG using amperometric immunosensors based on a conducting immunocomposite.* Analytica Chimica Acta, 1999. **396**(2-3): p. 181-188.

25. Kueng, A., C. Kranz, and B. Mizaikoff, *Amperometric ATP biosensor based on polymer entrapped enzymes.* Biosensors and Bioelectronics, 2004. **19**(10): p. 1301-1307.

26. Eggins, B., *Analytical Techniques in the Sciences: Chemical Sensors and Biosensors.* John Wiley & Son, West Sussex, 2002.

27. Buerk, D., *Biosensors. Theory and Applications.* Technomic Publishing, Lancaster, 1993.

28. Vigassy, T., C.G. Huber, R. Wintringer, and E. Pretsch, *Monolithic Capillary-Based Ion-Selective Electrodes.* Analytical Chemistry, 2005. **77**(13): p. 3966-3970.

29. Guo, H., T. Yin, Q. Su, and W. Qin, *Potentiometric measurement of ascorbate by using a solvent polymeric membrane electrode.* Talanta, 2008. **75**(3): p. 851-855.

30. Smirnova, A., K. Mawatari, H. Takahashi, Y. Tanaka, H. Nakanishi, and T. Kitamori, *Development of a Micro-Potentiometric Sensor for the Microchip Analysis of Alkali Ions.* Analytical Sciences, 2009. **25**(12): p. 1397-1401.

31. Schoning, M.J. and A. Poghossian, *Recent advances in biologically sensitive field-effect transistors (BioFETs).* Analyst, 2002. **127**(9): p. 1137-1151.

32. Poghossian, A.S., *Method of fabrication of ISFET-based biosensors on an Si-SiO2-Si structure.* Sensors and Actuators B: Chemical, 1997. **44**(1-3): p. 361-364.

33. Kharitonov, A.B., M. Zayats, A. Lichtenstein, E. Katz, and I. Willner, *Enzyme monolayer-functionalized field-effect transistors for biosensor applications.* Sens. Actuators, B, 2000. **B70**(1-3): p. 222-231.

34. Yin, L.-T., J.-C. Chou, W.-Y. Chung, T.-P. Sun, K.-P. Hsiung, and S.-K. Hsiung, *Glucose ENFET doped with MnO2 powder.* Sensors and Actuators B: Chemical, 2001. **76**(1-3): p. 187-192.

35. Patolsky, F., B.P. Timko, G. Yu, Y. Fang, A.B. Greytak, G. Zheng, and C.M. Lieber, *Detection, Stimulation, and Inhibition of Neuronal Signals with High-Density Nanowire Transistor Arrays.* Science, 2006. **313**(5790): p. 1100-1104.

36. Lehmann, M., W. Baumann, M. Brischwein, H.-J. Gahle, I. Freund, R. Ehret, S. Drechsler, H. Palzer, M. Kleintges, U. Sieben, and B. Wolf, *Simultaneous measurement of cellular respiration and acidification with a single CMOS ISFET.* Biosensors and Bioelectronics, 2001. **16**(3): p. 195-203.

37. Cohen-Karni, T., Q. Qing, Q. Li, Y. Fang, and C.M. Lieber, *Graphene and Nanowire Transistors for Cellular Interfaces and Electrical Recording.* Nano Letters, 2010. **10**(3): p. 1098-1102.

38. Hafeman, D., J. Parce, and H. McConnell, *Light-addressable potentiometric sensor for biochemical systems.* Science, 1988. **240**(4856): p. 1182-1185.

39. Selvanayagam, Z.E., P. Neuzil, P. Gopalakrishnakone, U. Sridhar, M. Singh, and L.C. Ho, *An ISFET-based immunosensor for the detection of [beta]-Bungarotoxin.* Biosensors and Bioelectronics, 2002. **17**(9): p. 821-826.

40. Plekhanova, Y.V., A.N. Reshetilov, E.V. Yazynina, A.V. Zherdev, and B.B. Dzantiev, *A new assay format for electrochemical immunosensors: polyelectrolyte-based separation on membrane carriers combined with detection of peroxidase activity by pH-sensitive field-effect transistor.* Biosensors and Bioelectronics, 2003. **19**(2): p. 109-114.

41. Starodub, N.F., B.B. Dzantiev, V.M. Starodub, and A.V. Zherdev, *Immunosensor for the determination of the herbicide simazine based on an ion-selective field-effect transistor.* Analytica Chimica Acta, 2000. **424**(1): p. 37-43.

42. Tansil, N.C. and Z. Gao, *Nanoparticles in biomolecular detection.* Nano Today, 2006. **1**(1): p. 28-37.

43. Morales, A.M. and C.M. Lieber, *A Laser Ablation Method for the Synthesis of Crystalline Semiconductor Nanowires.* Science, 1998. **279**(5348): p. 208-211.

44. Hu, J., T.W. Odom, and C.M. Lieber, *Chemistry and Physics in One Dimension: Synthesis and Properties of Nanowires and Nanotubes.* Acc. Chem. Res., 1999. **32**: p. 435-445.

45. Liang, X. and S.Y. Chou, *Nanogap Detector Inside Nanofluidic Channel for Fast Real-Time Label-Free DNA Analysis.* Nano Letters, 2008. **8**(5): p. 1472-1476.

46. Li, C., M. Curreli, H. Lin, B. Lei, F.N. Ishikawa, R. Datar, R.J. Cote, M.E. Thompson, and C. Zhou, *Complementary Detection of Prostate-Specific Antigen Using In2O3 Nanowires and Carbon Nanotubes.* Journal of the American Chemical Society, 2005. **127**(36): p. 12484-12485.

47. Star, A., J.-C.P. Gabriel, K. Bradley, and G. Grüner, *Electronic Detection of Specific Protein Binding Using Nanotube FET Devices.* Nano Letters, 2003. **3**(4): p. 459-463.

48. Chen, R.J., S. Bangsaruntip, K.A. Drouvalakis, N. Wong Shi Kam, M. Shim, Y. Li, W. Kim, P.J. Utz, and H. Dai, *Noncovalent functionalization of carbon*

nanotubes for highly specific electronic biosensors. Proceedings of the National Academy of Sciences, 2003. **100**(9): p. 4984-4989.

49. So, H.-M., K. Won, Y.H. Kim, B.-K. Kim, B.H. Ryu, P.S. Na, H. Kim, and J.-O. Lee, *Single-Walled Carbon Nanotube Biosensors Using Aptamers as Molecular Recognition Elements.* Journal of the American Chemical Society, 2005. **127**(34): p. 11906-11907.

50. Star, A., E. Tu, J. Niemann, J.-C.P. Gabriel, C.S. Joiner, and C. Valcke, *Label-free detection of DNA hybridization using carbon nanotube network field-effect transistors.* Proceedings of the National Academy of Sciences of the United States of America, 2006. **103**(4): p. 921-926.

51. Tang, X., S. Bansaruntip, N. Nakayama, E. Yenilmez, Y.-l. Chang, and Q. Wang, *Carbon Nanotube DNA Sensor and Sensing Mechanism.* Nano Letters, 2006. **6**(8): p. 1632-1636.

52. Besteman, K., J.-O. Lee, F.G.M. Wiertz, H.A. Heering, and C. Dekker, *Enzyme-Coated Carbon Nanotubes as Single-Molecule Biosensors.* Nano Letters, 2003. **3**(6): p. 727-730.

53. Gruner, G. *Carbon nanotube transistors for biosensing applications*. 2005: SPIE.

54. Heinze, S., J. Tersoff, R. Martel, V. Derycke, J. Appenzeller, and P. Avouris, *Carbon Nanotubes as Schottky Barrier Transistors.* Physical Review Letters, 2002. **89**(10): p. 106801.

55. Ma, D.D.D., C.S. Lee, F.C.K. Au, S.Y. Tong, and S.T. Lee, *Small-Diameter Silicon Nanowire Surfaces.* Science, 2003. **299**(5614): p. 1874-1877.

56. Wu, Y., Y. Cui, L. Huynh, C.J. Barrelet, D.C. Bell, and C.M. Lieber, *Controlled Growth and Structures of Molecular-Scale Silicon Nanowires.* Nano Letters, 2004. **4**(3): p. 433-436.

57. Tian, B., P. Xie, T.J. Kempa, D.C. Bell, and C.M. Lieber, *Single-crystalline kinked semiconductor nanowire superstructures.* Nat Nano, 2009. **4**(12): p. 824-829.

58. Cui, Y., X. Duan, J. Hu, and C.M. Lieber, *Doping and Electrical Transport in Silicon Nanowires.* The Journal of Physical Chemistry B, 2000. **104**(22): p. 5213-5216.

59. Jin, S., D. Whang, M.C. McAlpine, R.S. Friedman, Y. Wu, and C.M. Lieber, *Scalable Interconnection and Integration of Nanowire Devices without Registration.* Nano Letters, 2004. **4**(5): p. 915-919.

60. PN, B., *Handbook of Chemical and Biological Sensors.* Taylor RF, Schultz JS (Eds), IOP Publishing, Philadelphia, USA, 1996.

61. HU, W., et al.;, *Lithographically Defined Si Nanowire Field Effect Transistors for Biochemical Sensing.* IEEE International Conference on Nanotechnology, 2008(3): p. 1-4.

62. Regonda, S., M. Aryal, and W. Hu, *Stability of HSQ nanolines defined by e-beam lithography for Si nanowire field effect transistors*. Vol. 26. 2008: AVS. 2247-2251.

63. Cui, Y., Q. Wei, H. Park, and C.M. Lieber, *Nanowire Nanosensors for Highly Sensitive and Selective Detection of Biological and Chemical Species.* Science, 2001. **293**(5533): p. 1289-1292.

64. Lin, T.-W., P.-J. Hsieh, C.-L. Lin, Y.-Y. Fang, J.-X. Yang, C.-C. Tsai, P.-L. Chiang, C.-Y. Pan, and Y.-T. Chen, *Label-free detection of protein-protein interactions using a calmodulin-modified nanowire transistor.* Proceedings of the National Academy of Sciences, 2009.

65. Hahm, J.-i. and C.M. Lieber, *Direct Ultrasensitive Electrical Detection of DNA and DNA Sequence Variations Using Nanowire Nanosensors.* Nano Letters, 2003. **4**(1): p. 51-54.

66. Patolsky, F., B.P. Timko, G. Zheng, and C.M. Lieber, *Nanowire-Based Nanoelectronic Devices in the Life Sciences.* MRS Bull, 2007. **32**: p. 142-149.

67. Lin, M.C., C.J. Chu, L.C. Tsai, H.Y. Lin, C.S. Wu, Y.P. Wu, Y.N. Wu, D.B. Shieh, Y.W. Su, and C.D. Chen, *Control and Detection of Organosilane Polarization on Nanowire Field-Effect Transistors.* Nano Letters, 2007. **7**(12): p. 3656-3661.

68. Patolsky, F., G. Zheng, and C.M. Lieber, *Fabrication of silicon nanowire devices for ultrasensitive, label-free, real-time detection of biological and chemical species.* Nat. Protocols, 2006. **1**(4): p. 1711-1724.

69. Pennelli, G., *Top down fabrication of long silicon nanowire devices by means of lateral oxidation.* Microelectronic Engineering, 2009. **86**(11): p. 2139-2143.

70. Wagner, R.S. and W.C. Ellis, *VAPOR-LIQUID-SOLID MECHANISM OF SINGLE CRYSTAL GROWTH.* Applied Physics Letters, 1964. **4**(5): p. 89-90.

71. Huang, Y., X. Duan, Q. Wei, and C.M. Lieber, *Directed Assembly of One-Dimensional Nanostructures into Functional Networks.* Science, 2001. **291**(5504): p. 630-633.

72. Whang, D., S. Jin, Y. Wu, and C.M. Lieber, *Large-Scale Hierarchical Organization of Nanowire Arrays for Integrated Nanosystems.* Nano Letters, 2003. **3**(9): p. 1255-1259.

73. Li, X., L. Zhang, X. Wang, I. Shimoyama, X. Sun, W.-S. Seo, and H. Dai, *Langmuir−Blodgett Assembly of Densely Aligned Single-Walled Carbon Nanotubes from Bulk Materials.* Journal of the American Chemical Society, 2007. **129**(16): p. 4890-4891.

74. Tao, A., F. Kim, C. Hess, J. Goldberger, R. He, Y. Sun, Y. Xia, and P. Yang, *Langmuir−Blodgett Silver Nanowire Monolayers for Molecular Sensing Using Surface-Enhanced Raman Spectroscopy.* Nano Letters, 2003. **3**(9): p. 1229-1233.

75. Yu, G., A. Cao, and C.M. Lieber, *Large-area blown bubble films of aligned nanowires and carbon nanotubes.* Nat Nano, 2007. **2**(6): p. 372-377.

76. Freer, E.M., O. Grachev, X. Duan, S. Martin, and D.P. Stumbo, *High-yield self-limiting single-nanowire assembly with dielectrophoresis.* Nat Nano, 2010. **5**(7): p. 525-530.

77. Dong, L., J. Bush, V. Chirayos, R. Solanki, J. Jiao, Y. Ono, J.F. Conley, and B.D. Ulrich, *Dielectrophoretically Controlled Fabrication of Single-Crystal Nickel Silicide Nanowire Interconnects.* Nano Letters, 2005. **5**(10): p. 2112-2115.

78. Motayed, A., M. He, A.V. Davydov, J. Melngailis, and S.N. Mohammad, *Simple model for dielectrophoretic alignment of gallium nitride nanowires.* Journal of Vacuum Science & Technology B: Microelectronics and Nanometer Structures, 2007. **25**(1): p. 120-123.

79. Raychaudhuri, S., S.A. Dayeh, D. Wang, and E.T. Yu, *Precise Semiconductor Nanowire Placement Through Dielectrophoresis.* Nano Letters, 2009. **9**(6): p. 2260-2266.

80. Fan, Z., J.C. Ho, Z.A. Jacobson, R. Yerushalmi, R.L. Alley, H. Razavi, and A. Javey, *Wafer-Scale Assembly of Highly Ordered Semiconductor Nanowire Arrays by Contact Printing.* Nano Letters, 2007. **8**(1): p. 20-25.

81. Stern, E., R. Wagner, F.J. Sigworth, R. Breaker, T.M. Fahmy, and M.A. Reed, *Importance of the Debye Screening Length on Nanowire Field Effect Transistor Sensors.* Nano Letters, 2007. **7**(11): p. 3405-3409.

82. Zhang, G.-J., J.H. Chua, R.-E. Chee, A. Agarwal, S.M. Wong, K.D. Buddharaju, and N. Balasubramanian, *Highly sensitive measurements of PNA-DNA hybridization using oxide-etched silicon nanowire biosensors.* Biosensors and Bioelectronics, 2008. **23**(11): p. 1701-1707.

83. Lin, S.-P., C.-Y. Pan, K.-C. Tseng, M.-C. Lin, C.-D. Chen, C.-C. Tsai, S.-H. Yu, Y.-C. Sun, T.-W. Lin, and Y.-T. Chen, *A reversible surface functionalized nanowire transistor to study protein-protein interactions.* Nano Today, 2009. **4**(3): p. 235-243.

84. Gao, X.P.A., G. Zheng, and C.M. Lieber, *Subthreshold Regime has the Optimal Sensitivity for Nanowire FET Biosensors.* Nano Letters, 2009. **10**(2): p. 547-552.

85. Zheng, G., F. Patolsky, Y. Cui, W.U. Wang, and C.M. Lieber, *Multiplexed electrical detection of cancer markers with nanowire sensor arrays.* Nat Biotech, 2005. **23**(10): p. 1294-1301.

86. Stern, E., J.F. Klemic, D.A. Routenberg, P.N. Wyrembak, D.B. Turner-Evans, A.D. Hamilton, D.A. LaVan, T.M. Fahmy, and M.A. Reed, *Label-free immunodetection with CMOS-compatible semiconducting nanowires.* Nature, 2007. **445**(7127): p. 519-522.

87. Sheehan, P.E. and L.J. Whitman, *Detection Limits for Nanoscale Biosensors.* Nano Letters, 2005. **5**(4): p. 803-807.

88. Nair, P.R. and M.A. Alam, *Performance limits of nanobiosensors*. Vol. 88. 2006: AIP. 233120.

89. Li, Z., Y. Chen, X. Li, T.I. Kamins, K. Nauka, and R.S. Williams, *Sequence-Specific Label-Free DNA Sensors Based on Silicon Nanowires.* Nano Letters, 2004. **4**(2): p. 245-247.

90. Berg, H.C., *Random Walks in Biology.* Princeton University Press, Princeton, 1993.

91. Squires, T.M., R.J. Messinger, and S.R. Manalis, *Making it stick: convection, reaction and diffusion in surface-based biosensors.* Nat Biotech, 2008. **26**(4): p. 417-426.

92. Bloomfield, V.A., D.M. Crothers, and I.T.J. Tinoco, *Nucleic Acids: Structures, Properties, and Functions.* University Science Books, Sausalito, CA, 2000.

93. Fritz, J., E.B. Cooper, S. Gaudet, P.K. Sorger, and S.R. Manalis, *Electronic detection of DNA by its intrinsic molecular charge.* Proceedings of the National Academy of Sciences, 2002. **99**(22): p. 14142-14146.

94. Bird, R.B., W.E. Stewart, and E.N. Lightfoot, *Transport Phenomena, edn. 2.* Wiley, New York, 2002.

95. Leal, L.G., *Advanced Transport Phenomena: Fluid Mechanics and Convective Transport Processes.* Cambridge University Press, Cambridge, 2007.

96. Newman, J., *The Fundamental Principles of Current Distribution and Mass Transport in Electrochemical Cells.* Electroanalytical Chemistry, 1973. **6**: p. 279-297.

97. Go, J. and M.A. Alam, *Statistical interpretation of "femtomolar" detection*. Vol. 95. 2009: AIP. 033110.

98. Butt, N.Z., P.D. Yoder, and M.A. Alam, *Soft Error Trends and New Physical Model for Ionizaing Dose Effects in Double Gate Z-RAM Cell.* IEEE Trans. Nucl. Sci, 2007. **54**: p. 2363-2370.

99. Condamin, S., O. Benichou, V. Tejedor, R. Voituriez, and J. Klafter, *First-passage times in complex scale-invariant media.* Nature, 2007. **450**(7166): p. 77-80.

100. Gao, Z., A. Agarwal, A.D. Trigg, N. Singh, C. Fang, C.-H. Tung, Y. Fan, K.D. Buddharaju, and J. Kong, *Silicon Nanowire Arrays for Label-Free Detection of DNA.* Analytical Chemistry, 2007. **79**(9): p. 3291-3297.

101. Zimmerman, W.B., *Electrochemical microfluidics.* Chemical Engineering Science, 2011. **66**(7): p. 1412-1425.

102. Kang, Y. and D. Li, *Electrokinetic motion of particles and cells in microchannels.* Microfluidics and Nanofluidics, 2009. **6**(4): p. 431-460.

103. Jones, T.B., *Electromechanics of Particles.* Cambridge University Press, New York, 1995.

104. Probstein, R.F., *Physicochemical hydrodynamics, 2nd edn.* Wiley, New York, 1994.

105. Reichmuth, D.S., S.K. Wang, L.M. Barrett, D.J. Throckmorton, W. Einfeld, and A.K. Singh, *Rapid microchip-based electrophoretic immunoassays for the detection of swine influenza virus.* Lab on a Chip, 2008. **8**(8): p. 1319-1324.

106. Huang, L.R., J.O. Tegenfeldt, J.J. Kraeft, J.C. Sturm, R.H. Austin, and E.C. Cox, *A DNA prism for high-speed continuous fractionation of large DNA molecules.* Nat Biotech, 2002. **20**(10): p. 1048-1051.

107. Toriello, N.M., E.S. Douglas, and R.A. Mathies, *Microfluidic Device for Electric Field-Driven Single-Cell Capture and Activation.* Analytical Chemistry, 2005. **77**(21): p. 6935-6941.

108. Ozkan, M., T. Pisanic, J. Scheel, C. Barlow, S. Esener, and S.N. Bhatia, *Electro-Optical Platform for the Manipulation of Live Cells†.* Langmuir, 2002. **19**(5): p. 1532-1538.

109. Morgan, H. and N. Green, *AC electrokinetics: colloids and nanoparticles.* Research Studies Press, Philadelphia, 2002.

110. Wang, L., L.A. Flanagan, N.L. Jeon, E. Monuki, and A.P. Lee, *Dielectrophoresis switching with vertical sidewall electrodes for microfluidic flow cytometry*. Lab on a Chip, 2007. **7**(9): p. 1114-1120.

111. Arnold, W., *Positioning and levitation media for the separation of biological cells.* IEEE Trans Ind Appl, 2001. **37**(5): p. 1468-1475.

112. Arai, F., A. Ichikawa, M. Ogawa, T. Fukuda, K. Horio, and K. Itoigawa, *High-speed separation system of randomly suspended single living cells by laser trap and dielectrophoresis.* Electrophoresis, 2001. **22**(2): p. 283-288.

113. Li, Y., C. Dalton, H.J. Crabtree, G. Nilsson, and K.V.I.S. Kaler, *Continuous dielectrophoretic cell separation microfluidic device.* Lab on a Chip, 2007. **7**(2): p. 239-248.

114. Borgatti, M., L. Altomare, M. Abonnec, E. Fabbri, N. Manaresi, G. Medoro, A. Romani, M. Tartagni, C. Nastruzzi, Di Croce S, A. Tosi, I. Mancini, R. Guerrieri, and R. Gambari, *Dielectrophoresisbased 'lab-on-a-chip' devices for programmable binding of microspheres to target cells.* Intl J Oncol, 2005. **27**(6): p. 1559-1566.

115. Magnus, S.J. and et al., *Contact-free single-cell cultivation by negative dielectrophoresis.* Journal of Physics D: Applied Physics, 2008. **41**(17): p. 175502.

116. Russel, W.B., Saville, D.A., Schowalter, W.R., *Colloidal Dispersions*. 1989: Cambridge University Press.

117. Ghosal, S., *Fluid mechanics of electroosmotic flow and its effect on band broadening in capillary electrophoresis.* Electrophoresis, 2004. **25**(2): p. 214-28.

118. Wang, W., F. Zhou, L. Zhao, J.-R. Zhang, and J.-J. Zhu, *Measurement of electroosmotic flow in capillary and microchip electrophoresis.* Journal of Chromatography A, 2007. **1170**(1-2): p. 1-8.

119. Green, N.G., A. Ramos, A. Gonzalez, H. Morgan, and A. Castellanos, *Fluid flow induced by non-uniform AC electric fields in electrolytes on microelectrodes III: Observation of streamlines and numerical simulation.* Physical Review E, 2002. **66**: p. 026305.

120. Nadal, F., ccedil, ois, F. Argoul, oise, P. Hanusse, B. Pouligny, and A. Ajdari, *Electrically induced interactions between colloidal particles in the vicinity of a conducting plane.* Physical Review E, 2002. **65**(6): p. 061409.

121. Yeh, S.-R., M. Seul, and B.I. Shraiman, *Assembly of ordered colloidal aggregrates by electric-field-induced fluid flow.* Nature, 1997. **386**(6620): p. 57-59.

122. Meng, L. and et al., *Particle Line Assembly/Patterning by Microfluidic AC Electroosmosis.* Journal of Physics: Conference Series, 2006. **34**(1): p. 589.

123. Chen, L., J. Ma, and Y. Guan, *Study of an electroosmotic pump for liquid delivery and its application in capillary column liquid chromatography.* Journal of Chromatography A, 2004. **1028**(2): p. 219-226.

124. Linan, J., J. Mikkelsen, K. Jae-Mo, D. Huber, Y. Shuhuai, Z. Lian, Z. Peng, J.G. Maveety, R. Prasher, J.G. Santiago, T.W. Kenny, and K.E. Goodson, *Closed-loop electroosmotic microchannel cooling system for VLSI circuits.* Components and Packaging Technologies, IEEE Transactions on, 2002. **25**(3): p. 347-355.

125. Chen, L., J. Choo, and B. Yan, *The microfabricated electrokinetic pump: a potential promising drug delivery technique.* Expert Opinion on Drug Delivery, 2007. **4**(2): p. 119-129.

126. Paul, P. and D. Rakestraw, *Electrokinetic high pressure hydraulic system.* US Patent 6,019,882, 2000.

127. Belosludtsev, Y., I. Belosludtsev, B. Iverson, S. Lemeshko, R. Wiese, M. Hogan, and T. Powdrill, *Nearly instantaneous, cation-independent, high selectivity nucleic acid hybridization to DNA microarrays.* Biochemical and Biophysical Research Communications, 2001. **282**(5): p. 1263-1267.

128. Liu, Y., W.K. Liu, T. Belytschko, N. Patankar, A.C. To, A. Kopacz, and J.H. Chung, *Immersed electrokinetic finite element method.* International Journal for Numerical Methods in Engineering, 2007. **71**(4): p. 379-405.

129. Liu, W.K., Y.L. Liu, D. Farrell, L. Zhang, X.S. Wang, Y. Fukui, N. Patankar, Y.J. Zhang, C. Bajaj, J. Lee, J.H. Hong, X.Y. Chen, and H.Y. Hsu, *Immersed finite element method and its applications to biological systems.* Computer Methods in Applied Mechanics and Engineering, 2006. **195**(13-16): p. 1722-1749.

130. Liu, Y.L., K. Oh, J.G. Bai, C.L. Chang, W. Yeo, J.H. Chung, K.H. Lee, and W.K. Liu, *Manipulation of nanoparticles and biomolecules by electric field and surface tension.* Computer Methods in Applied Mechanics and Engineering, 2008. **197**(25-28): p. 2156-2172.

131. Liu, Y.L., J.H. Chung, W.K. Liu, and R.S. Ruoff, *Dielectrophoretic assembly of nanowires.* Journal of Physical Chemistry B, 2006. **110**(29): p. 14098-14106.

132. Zhang, B. and A. Docoslis, *Accelerated virus capture to surfaces inside physiological media by using AC electrokinetic effects.* In: Proceedings of the COMSOL Multiphysics User's Conference, Boston, 2005.

133. Cheng, J., K. Sharp, and M.M. Mench, *Modeling electrode position of charged nanoparticles onto fuel cell coolant flow channel walls.* In: Proceedings of the COMSOL Multiphysics User's Conference, Boston, 2006.

134. Davison, S.M. and K.V. Sharp, *Implementation of ALE moving mesh for transient modeling of nanowire trajectories caused by electrokinetic forces.* In: Proceedings of the COMSOL Multiphysics User's Conference, Boston, 2006.

135. Nair, P.R. and M.A. Alam, *Design Considerations of Silicon Nanowire Biosensors.* Electron Devices, IEEE Transactions on, 2007. **54**(12): p. 3400-3408.

136. Asenov, A., A.R. Brown, J.H. Davies, S. Kaya, and G. Slavcheva, *Simulation of intrinsic parameter fluctuations in decananometer and nanometer-scale MOSFETs.* Electron Devices, IEEE Transactions on, 2003. **50**(9): p. 1837-1852.

137. Tian, R., S. Regonda, J. Gao, Y. Liu, and W. Hu, *Ultrasensitive protein detection using lithographically defined Si multi-nanowire field effect transistors.* Lab on a Chip, 2011. **11**(11): p. 1952-1961.

138. Sze, S.M., *Physics of Semiconductor Devices, Second Edition.* Wiley and Sons, NewYork, 1981.

139. Berg, J.M., J.L. Tymoczko, and L. Stryer, *Biochemistry, 5th edition.* W H Freeman, New York, 2002.

140. Wilkins, M.R. and K.L. Williams, *Cross-Species Protein Identification using Amino Acid Composition, Peptide Mass Fingerprinting, Isoelectric Point and Molecular Mass: A Theoretical Evaluation.* Journal of Theoretical Biology, 1997. **186**(1): p. 7-15.

141. Ramachandran, A., Q. Guo, S.M. Iqbal, and Y. Liu, *Coarse-Grained Molecular Dynamics Simulation of DNA Translocation in Chemically Modified Nanopores.* The Journal of Physical Chemistry B, 2011. **115**(19): p. 6138-6148.

Vita

Qingjiang Guo was born on October 9, 1987 to Xiangui Guo and Xiaolan Li, in Nanchang, the capital of Jiangxi Province in southeastern China. He attended both the most prestigious high school and university in the country, Nanchang No.2 Middle School and Huazhong University of Science and Technology. During undergraduate years, he enrolled in the Naval Architectural and Ocean Engineering Program and received systematical education in Finite Element Analysis of ship structures and ship design using AutoCAD. He obtained his B.S. degree in 2009 and then applied and was accepted into the M.S. Mechanical Engineering Program at Lehigh University, where his research was supervised and supported by the advisor Yaling Liu. In Dr. Liu's lab, he was trained to become a professional in the area of biosensing technologies and coauthored four publications. He also served as a Graduate Teaching Assistant for four semesters. Currently, he is submitting this thesis for an M.S. degree, and actively looking for opportunities to commercialize silicon nanowire sensing devices.